Divergence of trafficking and polarity mechanisms for PIN auxin transporters during land plant evolution

Han Tang[1#], Kuan-Ju Lu[2#], You-Liang Cheng[3], Shih-Long Tu[3], and Jiří Friml[1*]

1. Institute of Science and Technology Austria (ISTA), Am Campus 1, 3400 Klosterneuburg, Austria

2. Graduate Institute of Biotechnology, National Chung Hsing University, No. 145, Xingda Rd., South Dist., Taichung 40227, Taiwan, R.O.C.

3. Institute of Plant and Microbial Biology, Academia Sinica, 128 Sec. 2, Academia Rd, Nankang, Taipei 11529, Taiwan, R.O.C.

# Equal contribution, * Correspondence: jiri.friml@ista.ac.at

The author responsible for distribution of materials integral to the findings presented in this article in accordance with the policy described in the Instructions for Authors (https://academic.oup.com/plcell) is: Jiri Friml (jiri.friml@ista.ac.at).

Abstract (~200 words)

The phytohormone auxin and its directional transport through tissues play a fundamental role in plant development. This polar auxin transport relies on the PIN auxin exporters, whose polarization at the plasma membrane determines the overall direction of auxin flow. Hence, PIN polarization is crucial for development, but its evolution during the rise of developmental complexity in land plants remains unclear. Here, we investigated the evolution of PIN trafficking and polarization by comparing two model bryophytes, *Physcomitrella patens* and *Marchantia polymorpha*, with the angiosperm model *Arabidopsis thaliana*. All examined PINs show a conserved auxin export function, which is reflected by comparable bryophytic growth defects in overexpression lines. In bryophytes, bryophytic PINs polarize to filamentous apices, while Arabidopsis PINs distribute symmetrically on the membrane with additional intracellular puncta. In the Arabidopsis root epidermis, bryophytic PINs show no defined polarity. Pharmacological interference revealed a strong cytoskeleton dependence of bryophytic but not Arabidopsis PIN polarization, which, in contrast, strongly relies on Brefeldin A-sensitive trafficking. The divergence of PIN polarization and trafficking is also observed within the bryophyte clade and between tissues in individual species. These results collectively reveal a divergence of PIN trafficking and polarity mechanisms throughout land plant evolution and suggest co-evolution of PIN sequence-based and cell-based polarity mechanisms.

Introduction

Auxin is a crucial regulator of polarity and morphogenesis in land plants (Mockaitis and Estelle, 2008; Smit and Weijers, 2015; Kato et al., 2018; Leyser, 2018; Yu et al., 2022). The auxin concentration gradient through tissues coordinates a broad spectrum of plant development, ranging from embryogenesis to organ formation and tropic growth (Vanneste and Friml, 2009; Friml, 2021). The establishment of the auxin gradient relies on particular auxin transporters, including the efflux carriers PIN-FORMED (PINs). In different tissues, specific PINs are polarized at different domains of the cells, thus directly driving the directional auxin flow across tissues (Adamowski and Friml, 2015). Therefore, given the essential impact of auxin flow in various developmental processes, the function and polarization of PIN proteins are crucial for maintaining the correct patterns of plant growth (Sauer and Kleine-Vehn, 2019).

PINs are found in all land plants and can be traced back to charophytic green algae (Krecek et al., 2009; Skokan et al., 2019). The functional conservation of PIN proteins in the auxin transport has also been demonstrated by exogenously expressing PINs from the green algae *Klebsormidium flaccidum*, the moss *Physcomitrium (Physcomitrella) patens*, and the angiosperm *Arabidopsis thaliana* in transgenic plants and heterologous systems (Zourelidou et al., 2014; Skokan et al., 2019). Additionally, when exogenous PINs from charophytes or Arabidopsis are overexpressed in Physcomitrella, the transgenic plants show growth inhibition that resembles auxin deprivation phenotypes (Viaene et al., 2014; Lavy et al., 2016; Tao and Estelle, 2018; Skokan et al., 2019). Therefore, these observations support the idea that PIN-mediated polar auxin transport may

78 govern plant development since the emergence of land plants.

79 The mechanistic studies of PIN polarity regulation have been extensively
80 investigated in the angiosperm Arabidopsis model. Canonical PINs, featuring a
81 long hydrophilic loop between two transmembrane domains, are first delivered
82 via the ER-Golgi vesicle trafficking pathway to the plasma membrane (PM).
83 De-polymerization of actin filaments induces the accumulation of PIN-labelled
84 small intracellular puncta near the PM, but with no apparent PIN polarity defect
85 (Geldner et al., 2001; Glanc et al., 2018, 2019). Microtubules are involved in
86 the cytokinetic trafficking of PINs, but are not required for the polarity
87 establishment or maintenance at the PM of non-dividing cells (Geldner et al.,
88 2001; Kleine-Vehn et al., 2008b; Glanc et al., 2019). Notably, the disruption of
89 both cytoskeleton networks delays, but does not abolish AtPIN2 polarization in
90 Arabidopsis epidermal cells (Glanc et al., 2019). This suggests that the
91 cytoskeleton networks are involved, but not exclusively essential for PIN polar
92 trafficking, while other mechanisms contribute to the PIN polar localization.

93 Once PINs are present on the PM, different processes, such as reducing
94 lateral diffusion and enhanced protein clustering, coordinate to maintain the
95 polar localization of PINs (Kleine-Vehn et al., 2011; Li et al., 2021). Recycling
96 of PINs from and to the PM also reinforces their polarity (Sauer and
97 Kleine-Vehn, 2019). During the PM recycling, PINs are first internalized
98 through the clathrin-dependent endocytosis (Dhonukshe et al., 2007), and
99 endocytic PINs are subsequently sorted out via a GNOM ARF-GEF pathway
100 (guanine nucleotide exchange factor) (Steinmann et al., 1999; Kleine-Vehn et
101 al., 2008b; Narasimhan et al., 2021). The GNOM ARF–GEF was shown to
102 interact with *trans*-Golgi network/early endosome (TGN/EE) and thereby
103 regulate the recycling of PINs (Naramoto et al., 2014). In Arabidopsis, the

fungal toxin Brefeldin A (BFA) inhibits the return of PINs from endocytic vesicles by blocking GNOM functions through unknown mechanisms. It thus leads to the accumulation of PINs in an enlarged endomembrane system, the so-called BFA bodies (Geldner et al., 2001).

PIN polarization was also observed in the moss model *Physcomitrella patens*. Physcomitrella grows as filamentous protonemata with tip cell growth, and PpPINA- and PpPINB-GFP show polar localization at the tip of protonema cells (Bennett et al., 2014; Viaene et al., 2014). However, their polar localization is not robust in other species. When PpPINA and PpPINB are expressed in Arabidopsis epidermal cells, where AtPIN2 presents clear apical localization, both Physcomitrella PIN proteins are mislocalized at basal and apical sites (Zhang et al., 2019). Furthermore, PINs from the liverwort *Marchantia polymorpha* and the green algae *Klebsormidium flaccidum* are also mislocalized in epidermal cells of Arabidopsis (Zhang et al., 2019). These distinctive PIN localizations in different species suggest that mechanisms for PINs trafficking and polarization may have diversified after the emergence of land plants.

Despite the profound significance of PIN polarization and the resulting directional auxin transport for land plant development, PIN trafficking and polarization mechanisms are mainly derived from the angiosperm model *Arabidopsis thaliana*. This research conducted a cross-species investigation to elucidate mechanisms and evolution of PIN trafficking and polarization by comparing two model bryophytes, *Physcomitrella patens* and *Marchantia polymorpha* with the model angiosperm *Arabidopsis thaliana*. In bryophytes and Arabidopsis, endogenous PINs show different trafficking and polarization patterns in a range of tissues, suggesting that tissues may utilize diverse

130 trafficking pathways for PIN localization. Pharmacological interference of
131 known Arabidopsis trafficking mechanisms further suggests that bryophytes
132 employ a different trafficking machinery for PIN polarization. Furthermore,
133 Arabidopsis PINs cannot be recruited by bryophyte trafficking pathways and
134 *vice versa*, confirming a species specificity for PIN polarity regulations. Overall,
135 this study revealed the divergence of PIN trafficking and polarity mechanisms
136 between bryophytes and angiosperms.
137

138 **Results**

139 **Physcomitrella PINs are polarized via different cytoskeleton-dependent**
140 **trafficking pathways**

141 Physcomitrella has a filamentous protonema stage and a leafy gametophore
142 stage in its life cycle. The polarization of PpPINA and PpPINB at the tips of
143 filamentous protonema cells has been demonstrated before (Viaene et al.,
144 2014). However, the underlying mechanism and whether it engages the same
145 trafficking pathways for the polarization of PINs in angiosperms, such as
146 Arabidopsis, remains unclear.

147 A stable Physcomitrella transgenic line carrying PpPINA genomic DNA
148 fused with GFP driven by its promoter (PpPINA-GFP) was used as the
149 standard model line throughout this research. However, we used a
150 constitutively over expressor maize actin promoter to drive PpPINB-GFP since
151 its expression under the *PpPINB* promoter is undetectable (Viaene et al.,
152 2014).

153 We observed the PpPINA-GFP localized at the PM of the protonema tip
154 with a clear polarity (Fig. 1A). Interestingly, PpPINB-GFP showed different
155 polarization patterns from PpPINA-GFP. In addition to a PM localization at the

156 filament tip, most of the PpPINB-GFP signal was accumulated at the dome
157 area of the protonema cell with a cytosolic diffusion (Fig. 1B). To examine
158 whether the polar localization of PpPINs appears in multicellular tissues, we
159 also observed their localizations in gametophores. In gametophytic leaves,
160 both PpPINA- and PpPINB-GFP were non-polarly distributed on the PM with
161 additional cytosolic puncta (Fig. S1).

162 Next, we examined the role of the cytoskeleton networks in the
163 polarization of PpPINs. To disrupt actin filaments or microtubules,
164 Physcomitrella tissues were treated with Latrunculin B (LatB) or Oryzalin (Ory),
165 respectively. Surprisingly, the abolishment of actin filaments resulted in the
166 hyper-polarization of PpPINA-GFP (Fig. 1A, 1C), accumulating at a focal locus
167 to the very tip of the cell (Fig. 1C-D). The disruption of microtubules resulted in
168 less accumulation of PpPINA-GFP at the tip of protonemata, and the
169 PpPINA-GFP appeared to be detached from the PM (Fig. 1A, 1C). Notably,
170 none of the drug treatments affected the polar localization of PpPINB-GFP (Fig.
171 1B). This result suggests that PpPINA and PpPINB are polarized through
172 different trafficking pathways in moss.

173

174 **Arabidopsis AtPIN1 and AtPIN2 are not polarized in Physcomitrella**

175 The intriguing divergence between PpPINA-GFP and PpPINB-GFP
176 polarization mechanisms prompted us to test whether it is a species-specific
177 mechanism. To achieve this, we generated Physcomitrella transgenic lines,
178 carrying Arabidopsis AtPIN1- and AtPIN2-GFP driven by *XVE* inducible
179 promoter (Fig. S2) (Kubo et al., 2013). In protonemata, both AtPIN1-GFP and
180 AtPIN2-GFP showed an even distribution on the PM without apparent polarity,
181 but they also displayed numerous small intracellular puncta (Fig. 1E, S3). The

182 dependency of the cytoskeletons was tested with LatB or Ory treatments,
183 however, no obvious effects on AtPIN1-GFP and AtPIN2-GFP PM localization
184 and cytosolic puncta were observed (Fig. 1E, S3). These observations indicate
185 that Arabidopsis PINs cannot be recruited into the moss polar trafficking
186 pathways and suggest a divergence of polarity mechanisms during the
187 evolution of land plants.
188
189 **Different modes of Brefeldin A action on trafficking in Physcomitrella**
190 BFA is a commonly used inhibitor (Geldner et al., 2001) to disrupt the PM
191 recycling of Arabidopsis PINs, resulting in the large intracellular BFA bodies
192 (Narasimhan et al., 2021). Therefore, we opted BFA to examine the PM
193 recycling of PpPINs in Physcomitrella. We first tested whether BFA has similar
194 effects in Physcomitrella by treating wild-type plants with BFA, followed by
195 labelling with the membrane dye FM4-64. Unlike in Arabidopsis, no clear BFA
196 bodies were observed (Fig. S4). Instead, the BFA-treated plants showed much
197 less internal FM4-64 particles compared to the DMSO control (Fig. S4), which
198 suggests an inhibitory effect of BFA on endocytosis in Physcomitrella.
199 Accordingly, PpPINA-GFP and PpPINB-GFP showed no striking changes in
200 subcellular distribution after BFA treatment (Fig. 2A). In contrast, AtPIN1-GFP
201 appeared to form larger intracellular puncta in response to BFA, resembling
202 BFA bodies in Arabidopsis (Fig. 2A).
203 The response of AtPIN1-GFP to BFA treatment suggests the presence of
204 a BFA-sensitive PM recycling in Physcomitrella. To further test whether
205 PpPINs and AtPINs undergo constitutive BFA-sensitive PM recycling, we
206 conducted fluorescence recovery after photobleaching (FRAP) experiments in
207 combination with BFA treatment. The PpPINA-GFP line was treated with the

208 protein synthesis inhibitor cycloheximide (CHX) with or without BFA present.
209 We performed FRAP analysis on a specific PM region near the filamentous tip
210 (Fig. 2B, white arrowheads). The recovery rate of PM-localized PpPINA-GFP
211 showed no difference in the presence or absence of BFA, suggesting that
212 PpPINA-GFP might not use the BFA-sensitive PM recycling pathway (Fig. 2B,
213 2D). In contrast to PpPINA-GFP, AtPIN1-GFP showed a slower recovery rate
214 when endocytosis was inhibited by BFA (Fig. 2C-2D), which is consistent with
215 the idea that AtPIN1-GFP might undergo the BFA-sensitive PM recycling in
216 Physcomitrella.

217 These observations show that Physcomitrella PINs do not use
218 BFA-sensitive PM recycling pathways, whereas heterologous expressed
219 Arabidopsis PINs do. This suggests that the functional domain of Arabidopsis
220 PINs can be recognized and recruited to a heterologous BFA-sensitive PM
221 recycling machinery in Physcomitrella.

222

223 **Overexpression of PINs inhibits the chloronema-caulonema transition in**
224 **Physcomitrella**

225 Because polarized PIN proteins act as auxin exporters to directly guide polar
226 auxin transport, they mediate many aspects of plant growth and development
227 (Friml, 2021). We therefore tested whether PpPINA- and PpPINB-GFP with
228 distinct polar localizations generate distinct gain-of-function phenotypes. To
229 investigate this, we generated overexpression lines by driving PpPINA- and
230 PpPINB-GFP under the control of the maize actin promoter. However, the
231 PpPINA-GFP over-expression line showed a robust cytoplasmic signal and
232 almost no signal on the PM (Fig. S5). To overcome this, we used the
233 pro*PINA*::PpPINA-GFP transgenic line, which is generated in a wild-type

234 background and carries two copies of *PpPINA*, and is thus an overexpression
235 plant.

236 During early development, Physcomitrella gradually transits its
237 filamentous protonemata from thicker/shorter chloronema cells with
238 perpendicular division planes to thinner/longer caulonema cells with oblique
239 division planes (Rensing et al., 2020). Overexpression of PpPINA- and
240 PpPINB-GFP led to similar defects in this chloronema-caulonema transition
241 with a shorter cell length of the subapical cell and a smaller division angle (Fig.
242 3A-C). No significant differences were observed between PpPINA- and
243 PpPINB-GFP overexpression. The inhibitory effect on the protonema transition
244 was also reflected in a smaller colony size in both PpPINA- and PpPINB-GFP
245 overexpression lines (Fig. 3D) (Viaene et al., 2014). This data indicates that
246 despite different localization patterns, Physcomitrella PINs produced
247 comparable gain-of-function phenotypes by inhibiting chloronema-caulonema
248 transition.

249 To test whether non-polar localized AtPIN1- and AtPIN2-GFP also result in
250 the same growth phenotypes in Physcomitrella, we analyzed the protonema
251 transition of inducible AtPIN1-GFP and AtPIN2-GFP lines. The
252 chloronema-caulonema transition was inhibited by overexpressing either
253 AtPIN1-GFP or AtPIN2-GFP (Fig. 3A-C). Furthermore, after induction, the
254 colony size of AtPIN1- and AtPIN2-GFP was much smaller than the wild-type
255 control, which showed a similar size to the DMSO treated wild-type plants (Fig.
256 3D). This result demonstrates the inhibitory effect of AtPINs overexpression on
257 the chloronema-caulonema transition. In addition to the protonema transition,
258 the overexpression of AtPIN1-GFP and AtPIN2-GFP led to wavy filaments and
259 multiple branching phenotypes, which was not observed in PpPINA- and

260 PpPINB-GFP overexpression lines (Fig. 3E).

261 These results thus indicate that regardless of their polarization, the
262 overexpression of PM-localized PINs likely leads to auxin depletion in
263 Physcomitrella filaments and thereby inhibits the chloronema-caulonema
264 transition.

265

266 **Marchantia MpPINZ is polarized at rhizoid tips but not in gemma cells**

267 The divergence of PIN polarity and trafficking between Physcomitrella and
268 Arabidopsis suggests an evolution deviation between bryophytes and
269 angiosperms. To confirm this notion, we looked at another bryophyte, the
270 liverwort *Marchantia polymorpha*. Gemmae are the asexual reproductive
271 progenies of Marchantia. After water imbibition, rhizoids emerge from the large
272 rhizoid precursor cells on the epidermis of the gemma. To analyze the
273 subcellular localization of the sole canonical PIN in Marchantia, MpPINZ, we
274 generated a pro*35S*::MpPINZ-GFP transgenic Marchantia line. Interestingly,
275 MpPINZ-GFP was localized on the PM with small intracellular puncta and no
276 apparent polarity in all gemma epidermal cells (Fig. 4A). However, when
277 gemmae were stimulated to grow rhizoids, the signal of MpPINZ-GFP
278 accumulated at the protrusion site of emerging rhizoids in the rhizoid precursor
279 cells (Fig. 4B, blue arrows). Later after their emergence, MpPINZ-GFP was
280 polarized at the tip of young rhizoids (Fig. 4C), whereas the signal diminished
281 when the rhizoids elongated.

282 We used the same pharmacological interference as in Physcomitrella to
283 investigate whether the MpPINZ-GFP PM localization or polarization relies on
284 the cytoskeleton networks and BFA-sensitive PM recycling. In gemmae, the
285 disruption of either microtubules or actin filaments did not affect the PM

286 localization, but the number and the size of intracellular puncta increased (Fig.
287 4D-F). In young rhizoids, MpPINZ-GFP remains polarized at the tip when actin
288 filaments were disrupted, while the disruption of microtubules resulted in the
289 dislocation of the polarized MpPINZ-GFP (Fig. 4D).

290 To test the BFA effect in Marchantia, we applied FM4-64 labeling to Tak-1
291 wild-type plants. The endocytic FM4-64 accumulated in significantly larger
292 intracellular compartments after BFA treatment (Fig. S6), suggesting that BFA
293 inhibits the return pathway of PM recycling in Marchantia as it does in
294 Arabidopsis. The BFA treatment of MpPINZ-GFP resulted in a small increase
295 of particles with larger size (Fig. 4D-F), indicating that MpPINZ-GFP does not
296 intensively go through the BFA-sensitive PM recycling. Consistent with the
297 notion, in young rhizoids, MpPINZ-GFP remained its polarization at the tip of
298 the filament with BFA treatment (Fig. 4D). Overall, these results reveal that
299 BFA-sensitive PM recycling and PIN polarity mechanisms also diverge within
300 the bryophyte clade.

301

302 **Arabidopsis PINs are not polarized in Marchantia**

303 We demonstrated that AtPIN1- and AtPIN2-GFP appeared non-polarized and
304 revealed cytosolic puncta in Physcomitrella. To investigate whether these
305 features are conserved in bryophytes, we introduced AtPIN1- and AtPIN2-GFP
306 driven by *35S* promoter into Marchantia. In gemma epidermal cells, the
307 AtPIN1-GFP showed non-polar PM localization with a high cytosolic signal (Fig.
308 5A). In emerging rhizoids, AtPIN1-GFP did not show visible polar localization
309 in rhizoid precursor cells (Fig. 5B). In young rhizoids, AtPIN1-GFP was evenly
310 distributed on the PM with homogenized cytosolic signals (Fig. 5C). The signal
311 of AtPIN2-GFP was much weaker but showed similar patterns as AtPIN1-GFP

312 in gemma epidermal cells (Fig. S7). However, we could not detect any signal of
313 AtPIN2-GFP in rhizoid cells, we therefore only used AtPIN1-GFP for further
314 study.

315 Next, we applied the same cytoskeleton-disruptive drugs to Marchantia
316 transgenic plants but we did not observe any effect on AtPIN1-GFP localization
317 in all examined tissues. We then tested whether the inhibition of BFA-sensitive
318 PM recylcing affects the localization of AtPIN1-GFP. With a range of different
319 concentrations and durations of BFA treatment, AtPIN1-GFP showed the same
320 PM and cytosolic signals as the non-treated control (Fig. S8), which indicates
321 that the non-polar localization of AtPIN1-GFP in Marchantia is insensitive to
322 BFA. These results demonstrate that Arabidopsis PINs in Marchantia do not
323 employ the same trafficking machinery as MpPINZ, and thus reinforce the
324 notion of divergence in PINs trafficking and polarity regulations between
325 bryophytes and angiosperms. Furthermore, the distinct localization patterns of
326 AtPIN-GFPs in moss and liverwort also verify the divergence of PIN trafficking
327 mechanisms within the bryophyte clade.

328

329 **Overexpression of PINs leads to a vertical growth of the thallus in**
330 **Marchantia**

331 Different localization patterns of MpPINZ- and AtPIN1-GFP in Marchantia
332 prompted us to investigate whether these differences result in divergent
333 growth phenotypes. The wild-type Marchantia has prostrate thalli; however,
334 with the overexpression of either MpPINZ-GFP or AtPIN-GFPs, the thallus
335 grew more vertically, as apparent from the side view (Fig. 6A). The angles
336 between the thallus and the horizontal agar medium were measured to
337 quantify the vertical growth (Fig. 6B). The overexpression of MpPINZ-GFP

338 caused the most striking phenotype, but the overexpression of AtPIN-GFPs
339 also resulted in a vertical growth that showed significant differences from the
340 wild-type. Notably, despite low expression levels, the overexpression of
341 AtPIN2-GFP still resulted in the vertical growth of the thallus. This data shows
342 that, similar to results in Physcomitrella, MpPINZ and AtPINs with different
343 subcellular localization, can trigger similar physiological responses.
344

345 **Bryophytic PINs utilize different trafficking mechanisms in Arabidopsis**

346 Since our results indicated that bryophytic PINs in their original species are
347 delivered to the PM through different trafficking pathways from the known
348 routes in Arabidopsis, we next addressed whether bryophytic PINs can utilize
349 Arabidopsis trafficking machinery. To analyze bryophytic PINs, we observed
350 the protein localization at epidermal cells of transgenic Arabidopsis plants
351 expressing pro*PIN2*::AtPIN2-, MpPINZ-, PpPINA-, and PpPINB-GFP (Zhang
352 et al., 2019). As previously described, AtPIN2-GFP showed apical localization
353 in the epidermal cells, while MpPINZ-GFP mainly localized on the basal side.
354 PpPINA-GFP localized on both the apical and basal sides, and PpPINB-GFP
355 presented not only PM localization but also intracellular signals (Fig. 7) (Zhang
356 et al., 2019).

357 The disruption of actin filaments by LatB resulted in an increasing
358 appearance of AtPIN2-GFP signals in the cell interior, while all bryophytic
359 PIN-GFPs showed hypersensitivity reflected by their accumulation in larger
360 intracellular compartments (Fig. 7). Ory was used to depolymerize
361 microtubules and caused a minor effect on AtPIN2-GFP and PpPINs, while the
362 MpPINZ-GFP in turn accumulated in large intracellular compartments (Fig. 7).
363 Following the inhibition of ARF GEF-mediated trafficking by the BFA, all three

364 bryophytic PINs accumulated in BFA bodies similar to AtPIN2-GFP. To verify
365 whether the PIN-GFP signal in the BFA bodies is recycled from the PM, we
366 inhibited the protein synthesis with CHX application prior to BFA treatment.
367 Surprisingly, the accumulated MpPINZ-GFP signal was not visible when CHX
368 was supplied, indicating that the intracellular accumulated signals of
369 MpPINZ-GFP was originated mainly from the pool of newly synthesized
370 proteins. Our results therefore suggest that the bryophytic PINs traffic to the
371 PM through divergent trafficking routes in Arabidopsis, and not all of them
372 undergo intensive BFA-sensitive PM recycling.
373

374 **Bryophytic PINs are polarized at the tip of initial root hairs**

375 As the polarity of bryophytic PINs in their original species mainly appeared at
376 the tip of filamentous tissues, we questioned whether the bryophytic PINs are
377 polarized in similar filamentous tissues in Arabidopsis; e.g. root hairs. We
378 observed bryophytic PIN-GFP signals in the initial and elongated root hairs.
379 Notably, all examined PIN-GFPs, including AtPIN2-GFP and bryophytic
380 PIN-GFPs, revealed a polar localization at the tip of initial root hairs. However,
381 the polarity of PIN signals disappeared in the elongated hairs (Fig. 8).

382 Next we tested whether this polar localization relies on the cytoskeleton
383 networks or is mediated through BFA-sensitive PM recycling. Surprisingly, all
384 treatments that disrupt cytoskeleton networks or PM recycling did not affect the
385 polarization of PINs on the initial root hairs (Fig. 8), which suggests that
386 different trafficking machinery are engaged in Arabidopsis epidermis and root
387 hairs.

388 In summary, these observations also confirm the divergence of trafficking
389 and PM localization mechanisms between bryophytes and angiosperms. In

390 addition, different trafficking pathways operate in distinct tissues, even within
391 individual species.
392
393 **Discussion**
394 **PIN polarity mechanisms display tissue-specific modifications**
395 In Arabidopsis, despite the functional redundancy of PIN proteins in auxin
396 transport, PINs show different polarization in different tissues (Vieten et al.,
397 2005). For example, AtPIN2 is apicalized in epidermal cells, while it is localized
398 on the basal side of young cortex cells (Kleine-Vehn et al., 2008a). The
399 observations imply that different tissues possess specific trafficking pathways
400 for the same PIN protein. In line with this, our results show that in filamentous
401 cells, e.g., protonemata in Physcomitrella, rhizoids in Marchantia, and root
402 hairs in Arabidopsis, endogenous PIN proteins are polarized at the tip of apical
403 cells. Nevertheless, the different dependency of cytoskeletons suggests that
404 the polarized trafficking mechanisms diversified between the three examined
405 species (Fig. 1, 4, 8). On the contrary, in multicellular tissues, e.g., leaves in
406 moss, thalli in Marchantia, and primary roots in Arabidopsis, the bryophytic PIN
407 proteins tend to distribute evenly on the PM (Fig. S1, 4, 7). Unlike in
408 filamentous tissues, the disruption of cytoskeleton networks shows minor
409 effect on the PINs distribution in multicellular tissues (Fig. S1, 4, 7). This data
410 shows that PIN polarity and trafficking mechanisms have evolved with specific
411 modifications in different tissues and cell types, both in angiosperms and
412 early-diverging land plants. This likely reflects different requirements for
413 directional auxin transport in different developmental contexts and implies a
414 co-evolution of PIN sequence-based signals and cell type-specific polar sorting
415 and trafficking mechanisms.

416

417 **Diversification of PIN polarity mechanisms during land plant evolution**

418 The core mechanisms for auxin biosynthesis, auxin signaling, and
419 PIN-mediated auxin transport are evolutionary conserved across land plants
420 (Kato et al., 2018; Sauer and Kleine-Vehn, 2019; Blazquez et al., 2020). Our
421 cross-species studies addressed to what extent the mechanism of PINs
422 trafficking is conserved during the evolution of land plants. It revealed that
423 exogenous PINs, such as Arabidopsis PINs in bryophytes and bryophytic PINs
424 in Arabidopsis, could be delivered to the PM but they cannot develop a correct
425 polarity and also show different sensitivities to interference with trafficking or
426 cytoskeletons (Fig. 1, 5, 7). These observations clearly show a divergence of
427 polarity mechanisms between bryophytic and vascular PINs. Notably,
428 endogenous PINs showed different responses to cytoskeletal disruption within
429 the bryophyte clade, indicating that trafficking pathways have already been
430 diversified between moss and liverwort (Fig. 1 and 4). Our study thus
431 demonstrates that PINs trafficking and polarity mechanisms are not conserved
432 throughout plant evolution. Instead, different plant species evolved specialized
433 pathways to deliver PINs and maintain their polarity at the PM. This is likely
434 linked to an increasing repertoire of auxin transport developmental roles
435 adopted with increasing morphological complexity during land plant evolution.

436

437 **Diversification of PIN trafficking mechanisms during land plant evolution**

438 Our comparative and interspecies complementation studies revealed different
439 cytoskeleton requirements for PIN polarization between bryophytes and
440 angiosperms. In Physcomitrella, both microtubules and actin filaments are
441 involved in the polarization of PpPINA-GFP to the tip of filaments (Fig. 1). In

442 Marchantia, only the disruption of microtubules disturbed the polar localization
443 of MpPINZ-GFP at the tip of young rhizoids (Fig. 4). In contrast, in Arabidopsis,
444 disruption of neither microtubules nor actin filaments would abolish the
445 AtPIN2-GFP apical localization (Glanc et al., 2019; Fig. 7). Instead, the
446 polarization of Arabidopsis PINs relies on several cellular processes, including
447 PM recycling, reduced lateral diffusion, and clustering (Kleine-Vehn et al., 2011;
448 Sauer and Kleine-Vehn, 2019). In line with this, we found that AtPIN1-GFP is
449 accumulated in larger intracellular puncta in BFA-treated Physcomitrella (Fig.
450 2), demonstrating the engagement of BFA-sensitive PM recycling routes in
451 AtPIN1 trafficking.

452 BFA was shown to preferentially cause intracellular accumulation of the
453 basal AtPIN2 but not the apical AtPIN2 (Kleine-Vehn et al., 2008b), which
454 supports that delivery to different polar domains at the PM may engage diverse
455 trafficking pathways. Notably, in the Arabidopsis epidermis, PpPINA-GFP
456 shows the same mislocalization patterns as the MpPINZ-GFP, but they display
457 distinct responses to the disruption of BFA-sensitive PM recycling (Fig. 7). This
458 observation implies that the distinct responses to BFA are probably due to not
459 only different make-up of trafficking pathways in different species, but also to
460 the differences in PIN molecules *per se*.

461 Overall, our data collectively show a strong sensitivity of bryophytic
462 PINs to the cytoskeletal disturbance and of Arabidopsis PINs to the BFA
463 treatment in different species. This finding suggests a gradual shift in the
464 dependence of PIN polarity and trafficking from the cytoskeleton-dependent
465 pathways towards the ARF GEF-mediated trafficking along the land plant
466 evolution.

467

468 **Co-evolution of polar trafficking mechanisms and PIN sequence-based**
469 **determinants**

470 One of the polarity maintenance mechanisms of PIN proteins is the ability to
471 recycle from and to the membrane (Kleine-Vehn et al., 2011). In Physcomitrella,
472 FRAP analysis demonstrated that PpPINA-GFP does not use the
473 BFA-sensitive PM recycling pathway, while AtPIN1-GFP does (Fig. 2). This
474 data demonstrates the BFA-sensitive PM recycling machinery already existed
475 in Physcomitrella. In Marchantia, BFA treatment led to the accumulation of
476 internalized FM4-64 dye in intracellular compartments (Fig. S6), which
477 resembles the BFA body in Arabidopsis, and thus again implicates that the
478 BFA-sensitive PM recycling is present in Marchantia. However, neither
479 MpPINZ-GFP nor AtPIN1-GFP accumulated in the BFA bodies in Marchantia
480 (Fig. 4, S8). These results demonstrate that BFA-sensitive, ARF
481 GEF-dependent PM recycling pathways emerged since bryophytes; however,
482 neither PpPINs nor MpPINZ employs these machineries in the original species,
483 despite the fact that PpPIN-GFPs can utilize them in Arabidopsis (Fig. 7).

484 These observations further confirm that both trafficking mechanisms and
485 relevant PIN sequences underwent a complex co-evolution during the gradual
486 rise of morphological complexity in land plants.

487

488 **Methods**

489 **Plant growth and transformation**

490 Arabidopsis seeds were surface sterilized and grown on 1/2 MS plates. After a
491 two-day stratification at 4°C, seedlings were grown under the long-day
492 condition (16 hours light, 8 hours dark) at 22°C with 100-120 μmol photons
493 $m^{-2}s^{-1}$ white light. For moss, all transgenic and WT plants were cultured on

494 BCD medium plates in a growth chamber at 24°C under the long-day condition
495 (16 hours light, 8 hours dark) with 35μmol photons $m^{-2}s^{-1}$ white light. For
496 Marchantia, WT and all transgenic plants were cultured on 1/2 B5 plates in a
497 growth chamber under the long-day condition (16 hours light, 8 hours dark) at
498 22°C with 50-60 μmol photons $m^{-2}s^{-1}$ white LED light.
499 All transgenic plants used in this study are listed in Supplemental Table 1.
500 Physcomitrella transgenic plants pro*PINA*::PINA-GFP and pro*ACT*::PINB-GFP
501 have been generated and verified as previously reported (Viaene et al., 2014),
502 and the inducible overexpression AtPIN1-GFP and AtPIN2-GFP lines were
503 generated as described in previous studies (Yamada et al., 2016; Tang et al.,
504 2020). In brief, the Gransden 2004 WT moss plants were freshly propagated
505 mosses and transformed via the PEG-mediated transformation (Nishiyama et
506 al., 2000). The transformants were selected under Hygromycin (20μg/mL), and
507 two independent transgenic lines were selected for imaging and analysis.
508 pro*35S*::MpPINZ-, AtPIN1-, and AtPIN2-GFP Marchantia plants were
509 generated via the Agrobacterium transformation method described before
510 (Kubota et al., 2013). In brief, the apical meristemic region of each
511 two-week-old Takaragaike-1 (Tak-1) thallus was removed and further cut into
512 eight pieces. After culturing on 1/2 B5 with 1% sucrose agar plates for 3 days,
513 the cut thalli were transferred to 50ml 0M51C medium with 200 μM
514 acetosyringone (4'-Hydroxy-3',5'-dimethoxyacetophenone) in 200ml flasks
515 with agitation at 130 rpm to coculture with OD_{600} = 1 density agrobacteria
516 harboring the target construct for another 3 days. The transformed thalli were
517 washed and plated on 1/2 B5 plates with proper antibiotic selection.
518 Independent T1 lines were isolated, and G1 lines from independent T1 lines
519 were generated by sub-cultivating single gemmalings, which emerged

520 asexually from a single initial cell (Shimamura, 2016). The next generation of
521 G1, called the G2 generation, was used for analyses.
522 Arabidopsis transgenic lines bearing bryophytic PIN-GFPs under *AtPIN2*
523 promoter control were generated and used as in a previous study (Zhang et al.,
524 2019). For root imaging, seeds were sown on 1/2 Murashige–Skoog (MS)
525 medium plates and kept at 4°C for 2 days and moved to the growth chamber to
526 culture vertically for another 4 days.
527
528 **Plasmid construction**
529 Plasmids and primers for construction and genotype confirmation are listed in
530 Supplemental Table 2. For transgenic lines with inducible overexpression by
531 moss, the cDNA of *AtPIN1* and *AtPIN2*, which inserted the *GFP* gene into the
532 hydrophilic loop at 461bp in *AtPIN1* and 736bp in *AtPIN2*, were amplified from
533 previously generated plasmids (Zhang et al., 2019) by PCR and cloned into
534 the gateway entry plasmid pENTR/D-TOPO. The fragments were sub-cloned
535 into the pPGX8 vector, which contains a pro*35S* driven β-estradiol inducible
536 XVE cassette (Nakaoka et al., 2012; Kubo et al., 2013; Floriach-Clark et al.,
537 2021) via a Gateway® LR reaction (Invitrogen) as the manufacture's
538 recommendation.
539 To generate a pro*35S*::MpPINZ-, AtPIN1-, and AtPIN2-GFP construct, the
540 cDNA of the target fragment containing proper *GFP* insertion were amplified
541 with the primers listed in Supplemental Table 2. The amplified fragments were
542 cloned into the pENTR/D-TOPO® vector (Invitrogen) with the protocol supplied
543 by the manufacturer. Plasmids with target genes were further sub-cloned into
544 the pMpGWB102 vector containing a *35S* promoter (Ishizaki et al., 2015) by
545 the Gateway® LR reaction (Invitrogen) as the manufacturer's

546 recommendation.

547

548 **Microscopy**

549 For moss observation, protonemata were cultured in glass-bottom dishes
550 covered by BCD agar medium for 6 – 7d. The live-cell imaging was then
551 performed on a Leica SP8X-SMD confocal microscope equipped with a hybrid
552 single-molecule detector (HyD) and an ultrashort pulsed white-light laser (WLL;
553 50%; 1 ps at 40 MHz frequency). The Leica Application Suite X was used as a
554 software platform, and imaging was conducted with a HC PL APO CS2
555 40x/1.20 water immersion objective. The following settings were used: scan
556 speed of 400 Hz, resolution of 1024 x 1024 pixels and standard acquisition
557 mode of the hybrid detector. The time-gating system was activated to avoid the
558 autofluorescence emitted from chloroplasts. For the filament growth assay, the
559 imaging dish was applied with FM4–64 (Invitrogen) solution for 10-30 mins,
560 and the 10x objective lens was used.

561 The FRAP analysis was performed under similar conditions with some
562 modifications. After capturing the first image as a “before” image, the HyD
563 detector was closed, and 2 lasers with full power were turned on. We
564 performed 8 – 10 times imaging capture with a 15-fold zoom-in that focused on
565 the bleaching area to ensure the bleaching efficiency. The bleaching area was
566 selected to cover at least one-third of the enriched signal on the membrane of
567 apical cells. After bleaching, a time series imaging was carried out in the same
568 setting as the “before” image with 1 min interval for another 8 minutes.

569 For Marchantia observation, gemmae were picked from a gemma cup and
570 transferred into a 24-well plate with 500 μl liquid 1/2 B5 medium. After culturing
571 in the growth chamber for 24 hours, gemmae from each sample were

572 transferred onto a 24mm x 50mm coverslip sandwich and observed on a slide
573 under Leica Stellaris 8 system with HyD detectors and the ultrashort pulsed
574 white-light laser (WLL; 70%; 1 ps at 40 MHz frequency). The Leica Application
575 Suite X was used as a software platform, and imaging was conducted with an
576 HC PL APO CS2 40x/1.20 water immersion objective. The following settings
577 were used: scan speed of 400 Hz and resolution of 1024 x 1024 pixels. For
578 GFP-containing images, a 488nm white light laser was selected, and the
579 detection range was set between 500nm to 525nm. For FM4-64 imaging, the
580 white light laser was set at 515nm for excitation, and the detection range was
581 set between 600nm to 700nm. The tau-gating model, harvesting photons with
582 1.0-10.0ns lifetime, was used for all Marchantia imaging to avoid
583 autofluorescence emitted from the chloroplasts. For the surface section
584 (rhizoid precursor cell observation), a 5μm-thick section was set using the
585 z-section method with auto-optimization spacing to capture rhizoids'
586 protrusion.
587 For Arabidopsis root imaging, 4-day-old seedlings of each indicated genotype
588 were used for fluorescence imaging. After treatment in the liquid MS medium
589 supplied with indicated chemicals, seedlings were carefully mounted on a slice
590 with growth medium and then placed into a chambered coverslip (Lab-Tek) for
591 imaging. For the root hair imaging, a 3μm Z-projection image with 1μm step
592 was taken around the medium plan of the root hair. All fluorescence imaging
593 was performed using a laser scanning confocal microscopy (Zeiss LSM800,
594 20x air lens). The default setting for GFP detection was applied with 488nm
595 excitation and 495-545nm emission.
596
597 **Images quantification**

598 All images were analyzed by Fiji (ImageJ, https://imagej.net/software/fiji/). For
599 the moss PpPINA-GFP polarization patterns at the tip of filaments, a line with
600 5px thickness was plotted along the PM from the blue to the green point, as
601 shown in Fig. 1. The representative images for the DMSO control and drug
602 treatments, obtained from the same imaging settings, were used to draw the
603 line, and the mean intensity along the line was shown. For the moss phenotype
604 analysis, mosses bearing inducible AtPIN1-GFP and AtPIN2-GFP were
605 cultivated in the imaging dish for 5 days, followed by 1μM β-estradiol induction
606 for another 3 days. For WT, pro*PINA*::PpPINA-GFP, and
607 pro*ACT*::PpPINB-GFP, tissues were cultivated for 8 days and cell outlines
608 were stained with FM4-64 for 10-30 mins. The line drawing function in Fiji was
609 used to measure the length of subapical cell, and the line was depicted
610 between the middle points of the two cell division planes. The angle
611 measurement function was applied to examine the angle between the first cell
612 division plane and horizontal cell outline for the division angle measurement.
613 For the Marchantia particle analysis, an individual cell was first selected
614 by the polygon selection tool and was further analyzed by the ComDet plugin
615 (https://imagej.net/plugins/spots-colocalization-comdet). We used 3 images for
616 each transgenic line and selected 20 cells for each image. We separately
617 detect particle sizes >3 pixels and >6 pixels for each cell. Other settings are
618 default.
619
620 **Genetic verification**
621 The genomic DNA of transformants was isolated by the
622 cetyltrimethylammonium bromide (CTAB) gDNA extraction (Schlink and Reski,
623 2002). In brief, moss tissues were harvested from one full plate and were

624 ground in liquid nitrogen. The ground tissues were then mixed and incubated
625 with a CTAB buffer, followed by the addition of chloroform. After centrifugation,
626 the supernatant was collected and precipitated with isopropanol at -20°C for
627 one hour. The PCR of the genomic DNA was performed with specific primers
628 listed in Supplemental Table S2.
629
630 **Pharmacological treatments**
631 To depolymerize microtubules and actin filaments, we used oryzalin (Sigma)
632 and latrunculin B (Sigma) to treat plants. The brefeldin A and cycloheximide
633 (Sigma) were used in the indicated conditions (Kleine-Vehn et al., 2008b). The
634 concentration and duration of treatment for different plants have been given in
635 numbers, and the conditions we used have been shown to efficiently
636 depolymerize cytoskeleton networks in different species (Baskin et al., 1994;
637 Baluska et al., 2001; Oda et al., 2009; Vidali et al., 2009; Glanc et al., 2019).
638 For Physcomitrella, the chemicals were diluted in a liquid BCD medium and
639 applied to the imaging dishes before imaging.
640 For Marchantia, G2 gemmae from transgenic plants were transferred into each
641 well of a 24-well plate containing 500μl liquid 1/2 B5 medium and cultured in
642 the growth chamber for 16 hours. The chemicals were diluted directly into the
643 medium prior to imaging at the time indicated in the text. Based on previous
644 studies, the concentration of Ory (Era et al., 2013) and LatB (Otani et al., 2018)
645 were selected.
646 For Arabidopsis, 4-days-old seedlings were submerged into the liquid MS
647 medium supplied with chemicals and then transferred to another agar medium
648 for imaging. 0.1% DMSO (Duchefa; 10 mM dimethylsulfoxide) was used as
649 control for all treatments.

650

651 **Moss colony growth assay**

652 For WT, overexpression of PpPINA- and PpPINB-GFP, the diameter of
653 20-day-old colonies cultivated on the same BCD medium agar plate was
654 measured. For the inducible AtPIN1- and AtPIN2-GFP lines, 10-day-old
655 colonies were transferred to another plate either with or without 1μM
656 β-estradiol (Sigma) for another 10 days. The diameter of each colony was then
657 measured. AtPIN1- and AtPIN2-GFP protonema phenotypes were imaged
658 using the Nikon Optiphot-2 Trinocular Transmitted light microscope after 6
659 days of induction.

660

661 **Marchantia thallus growth assay**

662 G2 gemmae were transferred onto 1/2 B5 agar plates and grew for 10 days.
663 Gemmae were imaged under a dissecting microscope (SZN71, LiWeng,
664 Taiwan) with a CCD camera (Polychrome M, LiWeng, Taiwan). For measuring
665 the vertical growth angle, an agar cube with an individual plant was cut out
666 from the plate and placed in the middle of a slide. The slide was put on the
667 surface of a laminar flow at a fixed distance to the edge, and images were
668 taken by an HTC U11 cell phone camera. The growth angle was further
669 measured by using ImageJ (https://imagej.net/software/fiji/).

670

671 **FRAP analysis**

672 For the FRAP analysis, images were captured at the medium plane and the
673 target regions were selected to focus on the PM signal and avoid intracellular
674 puncta. The intensity measurement was carried out with the Fiji program. The
675 mean intensity of the bleached area in the before image was measured and

676 normalized to 100%. The intensity of the same area at the time of serious
677 imaging after bleaching was measured and normalized according to the before
678 image to calculate the recovery rate.
679

680 **Author contributions and Acknowledgments**

681 H. T., K. J. L., and J. F. designed experiments. H. T. performed and analyzed
682 all the Physcomitrella and Arabidopsis related experiments with the help of Y.
683 L. C. and S. L. T.. K. J. L. performed and analyzed all the Marchantia related
684 experiments. H. T., K. J. L, and J. F. wrote the manuscript.

685 The authors would like to thank Dr A. Johnson and Ms Alexandra Mally for
686 their careful proofreading and Dr Y.Z. Zhang for kindly sharing At-, Pp-, and
687 MpPIN constructs. We also thank Dr T. Kohchi for sharing the pMpGWB102
688 vector (Addgene #68556; http://n2t.net/addgene:68556;
689 RRID:Addgene_68556).

690

691 **References**

692 Adamowski, M., and Friml, J. (2015). PIN-dependent auxin transport: action,
693 regulation, and evolution. Plant Cell 27, 20-32.
694 Baluska, F., Jasik, J., Edelmann, H.G., Salajova, T., and Volkmann, D. (2001).
695 Latrunculin B-induced plant dwarfism: Plant cell elongation is
696 F-actin-dependent. Dev Biol 231, 113-124.
697 Baskin, T.I., Wilson, J.E., Cork, A., and Williamson, R.E. (1994). Morphology
698 and microtubule organization in Arabidopsis roots exposed to oryzalin
699 or taxol. Plant Cell Physiol 35, 935-942.
700 Bennett, T.A., Liu, M.M., Aoyama, T., Bierfreund, N.M., Braun, M., Coudert, Y.,
701 Dennis, R.J., O'Connor, D., Wang, X.Y., White, C.D., Decker, E.L.,
702 Reski, R., and Harrison, C.J. (2014). Plasma membrane-targeted PIN
703 proteins drive shoot development in a moss. Curr Biol 24, 2776-2785.

704 Blazquez, M.A., Nelson, D.C., and Weijers, D. (2020). Evolution of Plant
705 Hormone Response Pathways. Annu Rev Plant Biol 71, 327-353.
706 Dhonukshe, P., Aniento, F., Hwang, I., Robinson, D.G., Mravec, J., Stierhof,
707 Y.D., and Friml, J. (2007). Clathrin-mediated constitutive endocytosis of
708 PIN auxin efflux carriers in Arabidopsis. Curr Biol 17, 520-527.
709 Era, A., Kutsuna, N., Higaki, T., Hasezawa, S., Nakano, A., and Ueda, T.
710 (2013). Microtubule stability affects the unique motility of F-actin in
711 Marchantia polymorpha. J Plant Res 126, 113-119.
712 Floriach-Clark, J., Tang, H., and Willemsen, V. (2021). Mosses: Accessible
713 Systems for Plant Development Studies. In Model Organisms in Plant
714 Genetics (IntechOpen.
715 Friml, J. (2021). Fourteen Stations of Auxin. Cold Spring Harb Perspect Biol 14,
716 a039859.
717 Geldner, N., Friml, J., Stierhof, Y.D., Jurgens, G., and Palme, K. (2001). Auxin
718 transport inhibitors block PIN1 cycling and vesicle trafficking. Nature
719 413, 425-428.
720 Glanc, M., Fendrych, M., and Friml, J. (2018). Mechanistic framework for
721 cell-intrinsic re-establishment of PIN2 polarity after cell division. Nat
722 Plants 4, 1082-1088.
723 Glanc, M., Fendrych, M., and Friml, J. (2019). PIN2 Polarity Establishment in
724 Arabidopsis in the Absence of an Intact Cytoskeleton. Biomolecules 9,
725 222.
726 Ishizaki, K., Nishihama, R., Ueda, M., Inoue, K., Ishida, S., Nishimura, Y.,
727 Shikanai, T., and Kohchi, T. (2015). Development of Gateway Binary
728 Vector Series with Four Different Selection Markers for the Liverwort
729 Marchantia polymorpha. PLoS One 10, e0138876.
730 Kato, H., Nishihama, R., Weijers, D., and Kohchi, T. (2018). Evolution of
731 nuclear auxin signaling: lessons from genetic studies with basal land
732 plants. J Exp Bot 69, 291-301.
733 Kleine-Vehn, J., Langowski, L., Wisniewska, J., Dhonukshe, P., Brewer, P.B.,
734 and Friml, J. (2008a). Cellular and molecular requirements for polar PIN
735 targeting and transcytosis in plants. Mol Plant 1, 1056-1066.
736 Kleine-Vehn, J., Dhonukshe, P., Sauer, M., Brewer, P.B., Wisniewska, J.,
737 Paciorek, T., Benkova, E., and Friml, J. (2008b). ARF GEF-dependent
738 transcytosis and polar delivery of PIN auxin carriers in Arabidopsis. Curr
739 Biol 18, 526-531.
740 Kleine-Vehn, J., Wabnik, K., Martiniere, A., Langowski, L., Willig, K., Naramoto,
741 S., Leitner, J., Tanaka, H., Jakobs, S., Robert, S., Luschnig, C.,

742 Govaerts, W., Hell, S.W., Runions, J., and Friml, J. (2011). Recycling,
743 clustering, and endocytosis jointly maintain PIN auxin carrier polarity at
744 the plasma membrane. Mol Syst Biol 7, 540.
745 Krecek, P., Skupa, P., Libus, J., Naramoto, S., Tejos, R., Friml, J., and
746 Zazimalova, E. (2009). The PIN-FORMED (PIN) protein family of auxin
747 transporters. Genome Biol 10, 249.
748 Kubo, M., Imai, A., Nishiyama, T., Ishikawa, M., Sato, Y., Kurata, T., Hiwatashi,
749 Y., Reski, R., and Hasebe, M. (2013). System for stable
750 beta-estradiol-inducible gene expression in the moss Physcomitrella
751 patens. PLoS One 8, e77356.
752 Kubota, A., Ishizaki, K., Hosaka, M., and Kohchi, T. (2013). Efficient
753 Agrobacterium-mediated transformation of the liverwort Marchantia
754 polymorpha using regenerating thalli. Biosci Biotechnol Biochem 77,
755 167-172.
756 Lavy, M., Prigge, M.J., Tao, S., Shain, S., Kuo, A., Kirchsteiger, K., and Estelle,
757 M. (2016). Constitutive auxin response in Physcomitrella reveals
758 complex interactions between Aux/IAA and ARF proteins. Elife 5,
759 e13325.
760 Leyser, O. (2018). Auxin Signaling. Plant Physiol 176, 465-479.
761 Li, H., von Wangenheim, D., Zhang, X., Tan, S., Darwish-Miranda, N.,
762 Naramoto, S., Wabnik, K., De Rycke, R., Kaufmann, W.A., Gutl, D.,
763 Tejos, R., Grones, P., Ke, M., Chen, X., Dettmer, J., and Friml, J. (2021).
764 Cellular requirements for PIN polar cargo clustering in Arabidopsis
765 thaliana. New Phytol 229, 351-369.
766 Mockaitis, K., and Estelle, M. (2008). Auxin receptors and plant development:
767 a new signaling paradigm. Annu Rev Cell Dev Biol 24, 55-80.
768 Nakaoka, Y., Miki, T., Fujioka, R., Uehara, R., Tomioka, A., Obuse, C., Kubo,
769 M., Hiwatashi, Y., and Goshima, G. (2012). An inducible RNA
770 interference system in Physcomitrella patens reveals a dominant role of
771 augmin in phragmoplast microtubule generation. Plant Cell 24,
772 1478-1493.
773 Naramoto, S., Otegui, M.S., Kutsuna, N., de Rycke, R., Dainobu, T.,
774 Karampelias, M., Fujimoto, M., Feraru, E., Miki, D., Fukuda, H., Nakano,
775 A., and Friml, J. (2014). Insights into the localization and function of the
776 membrane trafficking regulator GNOM ARF-GEF at the Golgi apparatus
777 in Arabidopsis. Plant Cell 26, 3062-3076.
778 Narasimhan, M., Gallei, M., Tan, S., Johnson, A., Verstraeten, I., Li, L.,
779 Rodriguez, L., Han, H., Himschoot, E., Wang, R., Vanneste, S.,

780 Sanchez-Simarro, J., Aniento, F., Adamowski, M., and Friml, J. (2021).
781 Systematic analysis of specific and nonspecific auxin effects on
782 endocytosis and trafficking. Plant Physiol 186, 1122-1142.
783 Nishiyama, T., Hiwatashi, Y., Sakakibara, I., Kato, M., and Hasebe, M. (2000).
784 Tagged mutagenesis and gene-trap in the moss, Physcomitrella patens
785 by shuttle mutagenesis. DNA Res 7, 9-17.
786 Oda, Y., Hirata, A., Sano, T., Fujita, T., Hiwatashi, Y., Sato, Y., Kadota, A.,
787 Hasebe, M., and Hasezawa, S. (2009). Microtubules regulate dynamic
788 organization of vacuoles in Physcomitrella patens. Plant Cell Physiol 50,
789 855-868.
790 Otani, K., Ishizaki, K., Nishihama, R., Takatani, S., Kohchi, T., Takahashi, T.,
791 and Motose, H. (2018). An evolutionarily conserved NIMA-related
792 kinase directs rhizoid tip growth in the basal land plant Marchantia
793 polymorpha. Development 145, dev154617.
794 Rensing, S.A., Goffinet, B., Meyberg, R., Wu, S.Z., and Bezanilla, M. (2020).
795 The Moss Physcomitrium (Physcomitrella) patens: A Model Organism
796 for Non-Seed Plants. Plant Cell 32, 1361-1376.
797 Sauer, M., and Kleine-Vehn, J. (2019). PIN-FORMED and PIN-LIKES auxin
798 transport facilitators. Development 146, dev.168088.
799 Schlink, K., and Reski, R. (2002). Preparing high-quality DNA from moss
800 (Physcomitrella patens). Plant Molecular Biology Reporter 20, 423-423.
801 Shimamura, M. (2016). Marchantia polymorpha: Taxonomy, Phylogeny and
802 Morphology of a Model System. Plant Cell Physiol 57, 230-256.
803 Skokan, R., Medvecka, E., Viaene, T., Vosolsobe, S., Zwiewka, M., Muller, K.,
804 Skupa, P., Karady, M., Zhang, Y., Janacek, D.P., Hammes, U.Z., Ljung,
805 K., Nodzynski, T., Petrasek, J., and Friml, J. (2019). PIN-driven auxin
806 transport emerged early in streptophyte evolution. Nat Plants 5,
807 1114-1119.
808 Smit, M.E., and Weijers, D. (2015). The role of auxin signaling in early embryo
809 pattern formation. Curr Opin Plant Biol 28, 99-105.
810 Steinmann, T., Geldner, N., Grebe, M., Mangold, S., Jackson, C.L., Paris, S.,
811 Galweiler, L., Palme, K., and Jurgens, G. (1999). Coordinated polar
812 localization of auxin efflux carrier PIN1 by GNOM ARF GEF. Science
813 286, 316-318.
814 Tang, H., Duijts, K., Bezanilla, M., Scheres, B., Vermeer, J.E.M., and
815 Willemsen, V. (2020). Geometric cues forecast the switch from two- to
816 three-dimensional growth in Physcomitrella patens. New Phytol 225,
817 1945-1955.

818 Tao, S., and Estelle, M. (2018). Mutational studies of the Aux/IAA proteins in
819 Physcomitrella reveal novel insights into their function. New Phytol 218,
820 1534-1542.
821 Vanneste, S., and Friml, J. (2009). Auxin: a trigger for change in plant
822 development. Cell 136, 1005-1016.
823 Viaene, T., Landberg, K., Thelander, M., Medvecka, E., Pederson, E., Feraru,
824 E., Cooper, E.D., Karimi, M., Delwiche, C.F., Ljung, K., Geisler, M.,
825 Sundberg, E., and Friml, J. (2014). Directional auxin transport
826 mechanisms in early diverging land plants. Curr Biol 24, 2786-2791.
827 Vidali, L., Rounds, C.M., Hepler, P.K., and Bezanilla, M. (2009).
828 Lifeact-mEGFP reveals a dynamic apical F-actin network in tip growing
829 plant cells. PLoS One 4, e5744.
830 Vieten, A., Vanneste, S., Wisniewska, J., Benkova, E., Benjamins, R.,
831 Beeckman, T., Luschnig, C., and Friml, J. (2005). Functional
832 redundancy of PIN proteins is accompanied by auxin-dependent
833 cross-regulation of PIN expression. Development 132, 4521-4531.
834 Yamada, M., Miki, T., and Goshima, G. (2016). Imaging Mitosis in the Moss
835 Physcomitrella patens. Methods Mol Biol 1413, 263-282.
836 Yu, Z., Zhang, F., Friml, J., and Ding, Z. (2022). Auxin signaling: Research
837 advances over the past 30 years. J Integr Plant Biol 64, 371-392.
838 Zhang, Y., Xiao, G., Wang, X., Zhang, X., and Friml, J. (2019). Evolution of fast
839 root gravitropism in seed plants. Nat Commun 10, 3480.
840 Zourelidou, M., Absmanner, B., Weller, B., Barbosa, I.C., Willige, B.C., Fastner,
841 A., Streit, V., Port, S.A., Colcombet, J., de la Fuente van Bentem, S.,
842 Hirt, H., Kuster, B., Schulze, W.X., Hammes, U.Z., and Schwechheimer,
843 C. (2014). Auxin efflux by PIN-FORMED proteins is activated by two
844 different protein kinases, D6 PROTEIN KINASE and PINOID. Elife 3,
845 e02860.

846

847 **Figure legends**

848

849 **Figure 1.** The divergence of PpPINs- and AtPIN1-GFP localization and
850 trafficking in Physcomitrella.

851 A, PpPINA-GFP is polarized to the tip of protonema, and the disruption of actin
852 filaments by Latrunculin B (LatB) caused its hyperpolarization. The disruption

853 of microtubules by Oryzalin (Ory) disturbed the polarization of PpPINA-GFP.
854 The blue dotted curves indicate the selected areas for intensity plot shows in
855 D.
856 B, PpPINB-GFP is polarized at the dome area of the protonema, but none of
857 the treatments influenced this localization.
858 C, Enlarged pictures derived from A with the focus on protonema tips. White
859 arrowheads indicate the hyperpolarization or the absence of PpPINA-GFP.
860 D, Relative intensity of PpPINA-GFP along the cell membrane between blue
861 and green dots as indicated in A.
862 E, After the induction of expression, AtPIN1-GFP is localized on the PM with
863 cytosolic puncta. The disruption of cytoskeletons did not affect the localization
864 of AtPIN1-GFP.
865 All images show the z-projection of 10 sections with a 1μm step. FM4-64 was
866 used as a PM marker. Treatments were conducted as indicated. All conditions
867 were verified in at least 2 independent lines and 3 independent experiments.
868 Scale bar = 10 μm.
869
870 **Figure 2.** PpPINs- and AtPIN1-GFP show different responses to BFA in
871 Physcomitrella**.**
872 A, Representative images of PpPINA-, PpPINB-, and AtPIN1-GFP localization
873 at the tips of protonema cells. The BFA treatment did not affect PpPINA- and
874 PpPINB-GFP. The white arrowheads indicate the accumulation of
875 AtPIN1-GFP in cytosolic puncta after the BFA treatment. All images show the
876 z-projection of 10 sections with a 1μm step.
877 B and C, Example images of FRAP analyses of PpPINA- and AtPIN1-GFP.
878 The white arrowheads depict the FRAP target regions. Single image was

879 captured with the medium focus on cell apices. Imaging details are descried in
880 Methods.
881 D, Quantification of the FRAP analysis. The recovery of AtPIN1-GFP signals
882 was reduced by BFA treatment, while PpPINA-GFP showed no recovery.
883 N=11 for each condition; each data point was collected from 3 independent
884 experiments. Scale bar = 10 μm, ***P<0.001; Student's *t*-test.
885
886 **Figure 3.** Overexpression of PpPIN- and AtPIN-GFPs inhibits the
887 chloronema-caulonema transition in Physcomitrella.
888 A, Representative protonema cells of the indicated genetic background. The
889 cell outline was stained with FM4-64. White arrowheads indicate the first cell
890 division plane, and the yellow double arrow indicates the cell length of the
891 subapical cell. Scale bar = 100 μm.
892 B and C, Quantitative results of the subapical cell length and the division angle
893 (Θ) of indicated lines, respectively.
894 D, The colony size of indicated lines. For inducible AtPIN-GFP lines, the
895 colony size under induction (β-estr) or mock (DMSO) condition was measured.
896 Four colonies were measured for each indicated line. ***P<0.001; Student's
897 *t*-test.
898 E, Growth phenotypes caused by the overexpression of AtPIN1- or
899 AtPIN2-GFP. White arrowheads indicate the multiple branches and wavy
900 filaments.
901
902 **Figure 4.** MpPINZ-GFP is only polarized at the tip of young rhizoids in
903 Marchantia.
904 A – C, The localization of MpPINZ-GFP in gemmae, emerging rhizoids, and

905 young rhizoids.

906 A, A middle section image as illustrated showing the even distribution of
907 MpPINZ-GFP on the PM of gemmae.

908 B, Representative image with a 5 μm thick Z-section at the gemma surface as
909 illustrated. Blue arrows indicate the accumulation of MpPINZ-GFP at tips of
910 emerging rhizoids in rhizoid precursor cells.

911 C, MpPINZ-GFP is polarized at the tip of young rhizoids.

912 D, The responses of MpPINZ-GFP to indicated treatments. MpPINZ-GFP is
913 localized on the PM with cytosolic puncta signals in gemmae.
914 De-polymerization of cytoskeleton networks caused more and larger cytosolic
915 puncta; BFA treatment resulted in the increase of puncta only with larger size.
916 MpPINZ-GFP is polarized at the tip of young rhizoids, and its polarization was
917 only abolished by Oryzalin treatment (white arrowhead).

918 E and F, Quantification of intracellular puncta larger than 3 pixels and 6 pixels.
919 20 cells were quantified in each image, and three images were used to
920 quantify for each treatment (N=60 in total). *P<0.05, **P<0.01, ***P<0.001;
921 Student's *t*-test.

922

923 **Figure 5.** Arabidopsis AtPIN1-GFP is not polarized in Marchantia.

924 A – C, The localization of AtPIN1-GFP in Marchantia gemmae, emerging
925 rhizoids, and young rhizoids. Imaging sections were obtained as illustrated in A
926 and B. The AtPIN1-GFP is localized on the PM and in the cytoplasm with no
927 apparent puncta signals in all examined tissues.

928

929 **Figure 6.** Overexpression of MpPINZ- and AtPIN-GFPs causes vertical growth
930 of Marchantia thalli.

931 A, Marchantia Tak-1 (WT) expands its thallus horizontally on the agar surface.
932 The overexpression of MpPINZ-, AtPIN1-, and AtPIN2-GFP showed vertical
933 thallus growth, which generated a large angle between the lower surface of the
934 thallus and the surface of the agar (θ).
935 B, The quantification of the thallus growth angle (θ) showed in A. N= 16 – 18
936 thali for each line. ***P<0.001; Student's *t*-test.
937
938 **Figure 7.** Bryophytic PINs and AtPIN2-GFP utilize different trafficking
939 mechanisms in Arabidopsis epidermal cells.
940 All PINs were translationally fused with GFP and expressed by the *AtPIN2*
941 promoter. De-polymerization of cytoskeleton networks caused mild
942 internalization of AtPIN2- and PpPINA-GFP, while PpPINB- and MpPINZ-GFP
943 showed strong responses with larger and more intracellular compartments.
944 BFA bodies were observed in all PIN-GFP lines with BFA treatment, while only
945 MpPINZ-GFP showed no BFA bodies in CHX+BFA treatment. Imaging details
946 are described in Methods.
947
948 **Figure 8.** Bryophytic PINs and AtPIN2-GFP are only polarized to the tip of
949 initial but not elongated root hairs.
950 All PIN-GFP lines show polarized signals at the tip of the initial root hair and
951 none of the indicated treatments disrupted their polarization. Note that the
952 polarization of the PIN-GFP signals were not observed in elongated root hairs.
953 All imaging details are described in Methods. The pixel values ranging from 0
954 to 255 are represented by the rainbow color.

Figure 1. The divergence of PpPINs- and AtPIN1-GFP localization and trafficking in Physcomitrella.

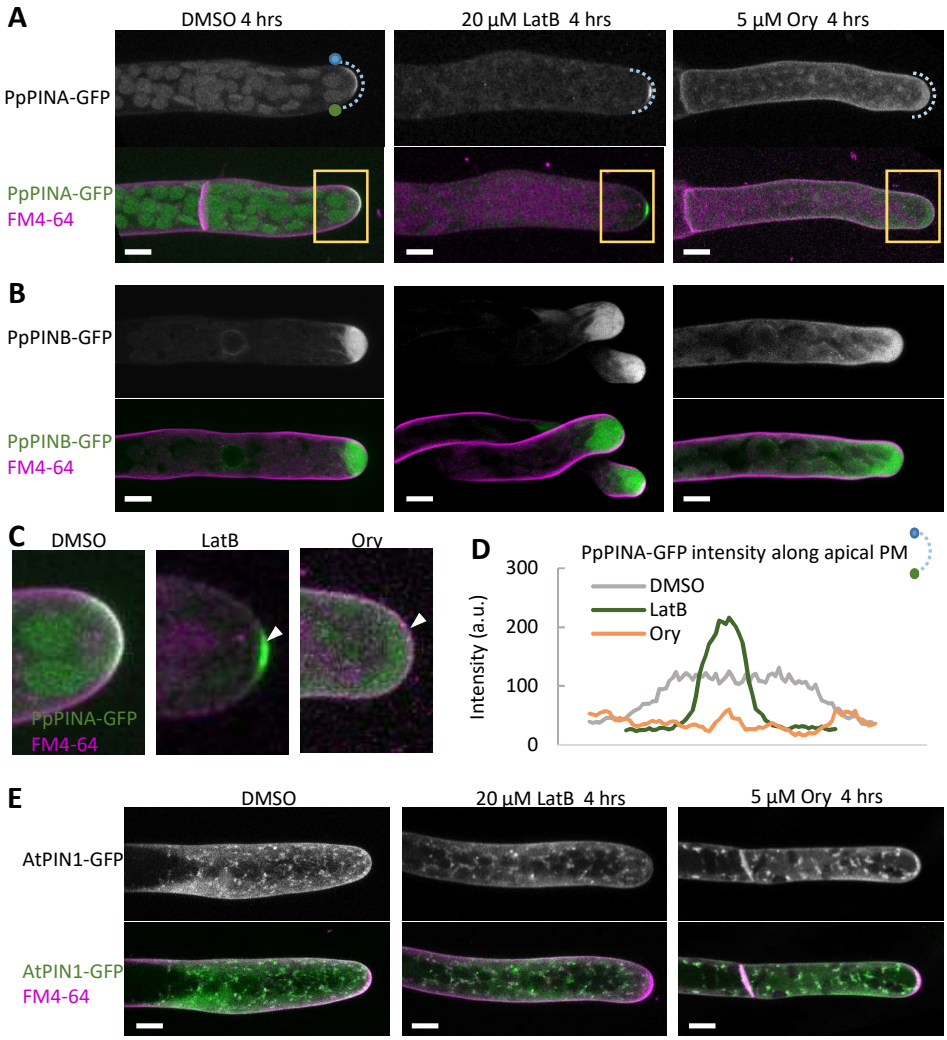

Figure 1. The divergence of PpPINs- and AtPIN1-GFP localization and trafficking in Physcomitrella.

A, PpPINA-GFP is polarized to the tip of protonema, and the disruption of actin filaments by Latrunculin B (LatB) caused its hyperpolarization. The disruption of microtubules by Oryzalin (Ory) disturbed the polarization of PpPINA-GFP. The blue dotted curves indicate the selected areas for intensity plot shows in D.
B, PpPINB-GFP is polarized at the dome area of the protonema, but none of the treatments influenced this localization.
C, Enlarged pictures derived from A with the focus on protonema tips. White arrowheads indicate the hyperpolarization or the absence of PpPINA-GFP.
D, Relative intensity of PpPINA-GFP along the cell membrane between blue and green dots as indicated in A.
E, After the induction of expression, AtPIN1-GFP is localized on the PM with cytosolic puncta. The disruption of cytoskeletons did not affect the localization of AtPIN1-GFP.
All images show the z-projection of 10 sections with a 1µm step. FM4-64 was used as a PM marker. Treatments were conducted as indicated. All conditions were verified in at least 2 independent lines and 3 independent experiments. Scale bar = 10 µm.

Figure 2. PpPINs- and AtPIN1-GFP show different responses to BFA in Physcomitrella.

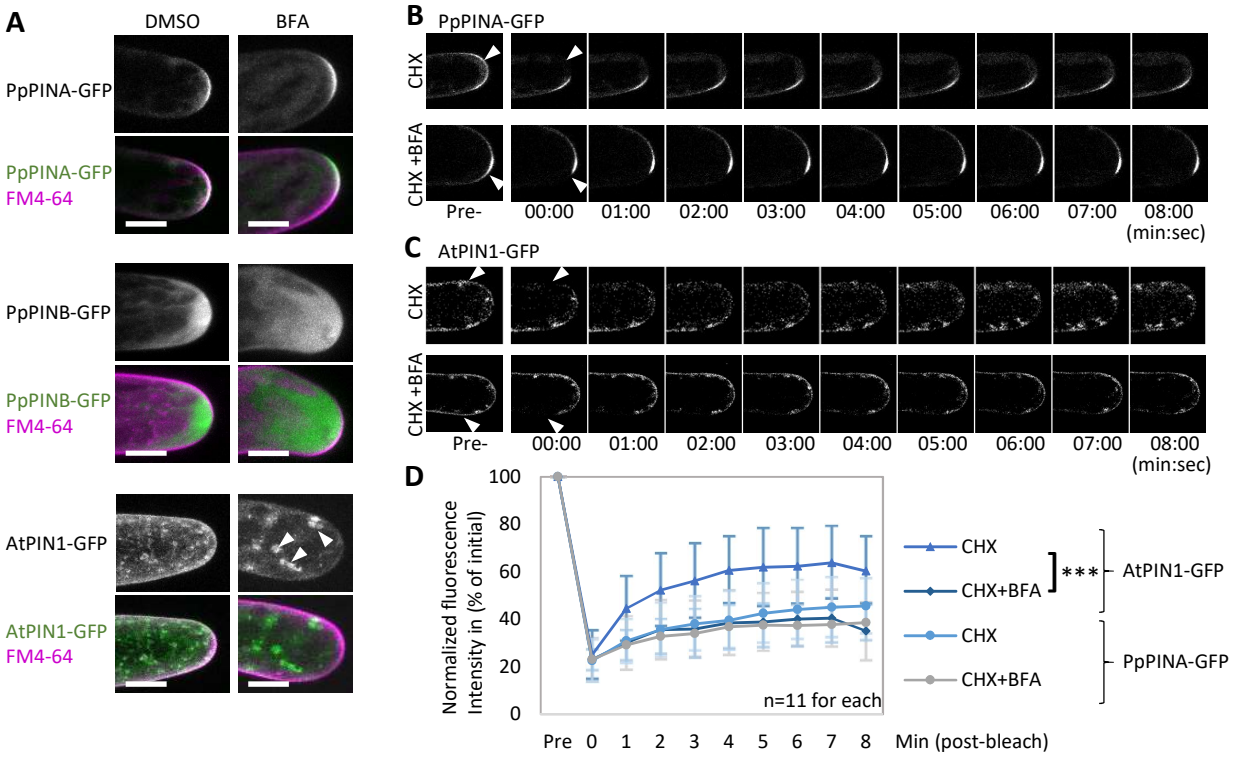

Figure 2. PpPINs- and AtPIN1-GFP show different responses to BFA in Physcomitrella**.**

A, Representative images of PpPINA-, PpPINB-, and AtPIN1-GFP localization at the tips of protonema cells. The BFA treatment did not affect PpPINA- and PpPINB-GFP. The white arrowheads indicate the accumulation of AtPIN1-GFP in cytosolic puncta after the BFA treatment. All images show the z-projection of 10 sections with a 1µm step.

B and C, Example images of FRAP analyses of PpPINA- and AtPIN1-GFP. The white arrowheads depict the FRAP target regions. Single image was captured with the medium focus on cell apices. Imaging details are descried in Methods.

D, Quantification of the FRAP analysis. The recovery of AtPIN1-GFP signals was reduced by BFA treatment, while PpPINA-GFP showed no recovery. N=11 for each condition; each data point was collected from 3 independent experiments. Scale bar = 10 µm, ***P<0.001; Student's *t*-test.

Figure 3. Overexpression of PpPIN- and AtPIN-GFPs inhibits the chloronema-caulonema transition in Physcomitrella.

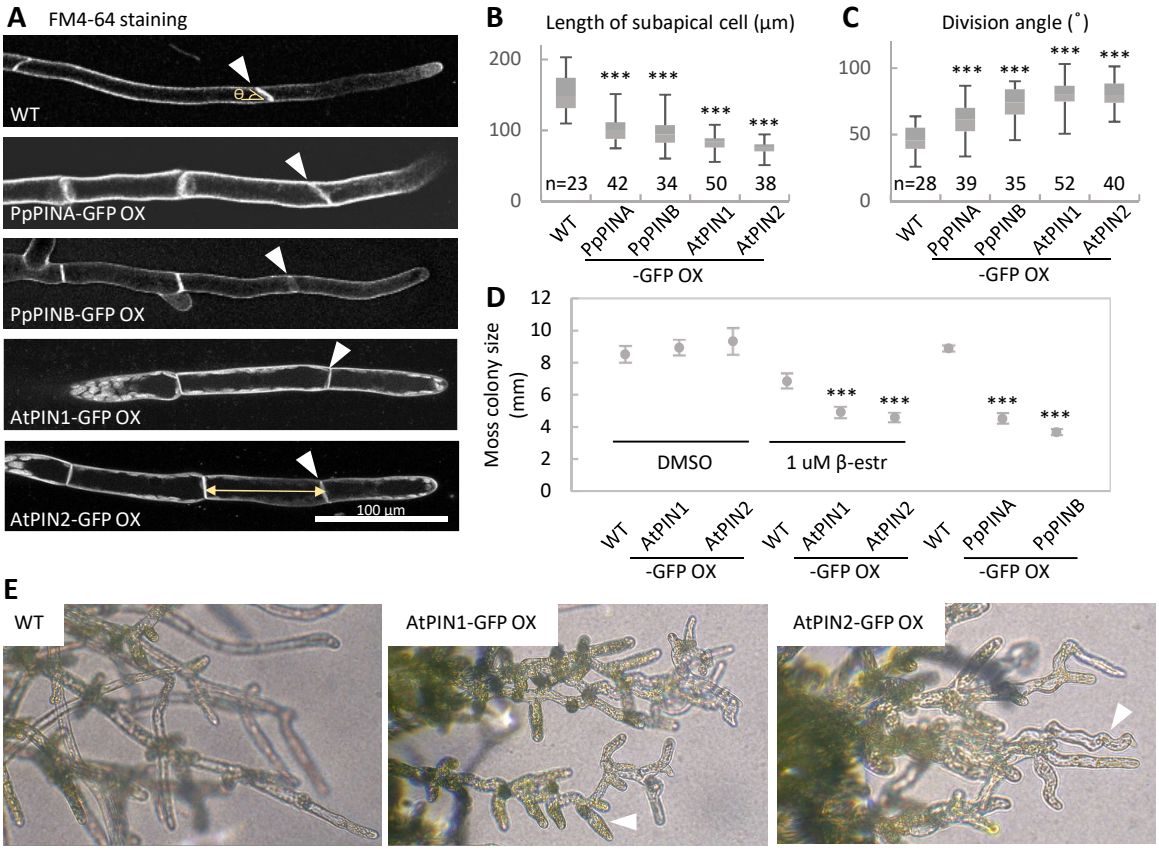

Figure 3. Overexpression of PpPIN- and AtPIN-GFPs inhibits the chloronema-caulonema transition in Physcomitrella.

A, Representative protonema cells of the indicated genetic background. The cell outline was stained with FM4-64. White arrowheads indicate the first cell division plane, and the yellow double arrow indicates the cell length of the subapical cell. Scale bar = 100 µm.
B and C, Quantitative results of the subapical cell length and the division angle (Θ) of indicated lines, respectively.
D, The colony size of indicated lines. For inducible AtPIN-GFP lines, the colony size under induction (β-estr) or mock (DMSO) condition was measured. Four colonies were measured for each indicated line. ***P<0.001; Student's *t*-test.
E, Growth phenotypes caused by the overexpression of AtPIN1- or AtPIN2-GFP. White arrowheads indicate the multiple branches and wavy filaments.

Figure 4. MpPINZ-GFP is only polarized at the tip of young rhizoids in Marchantia.

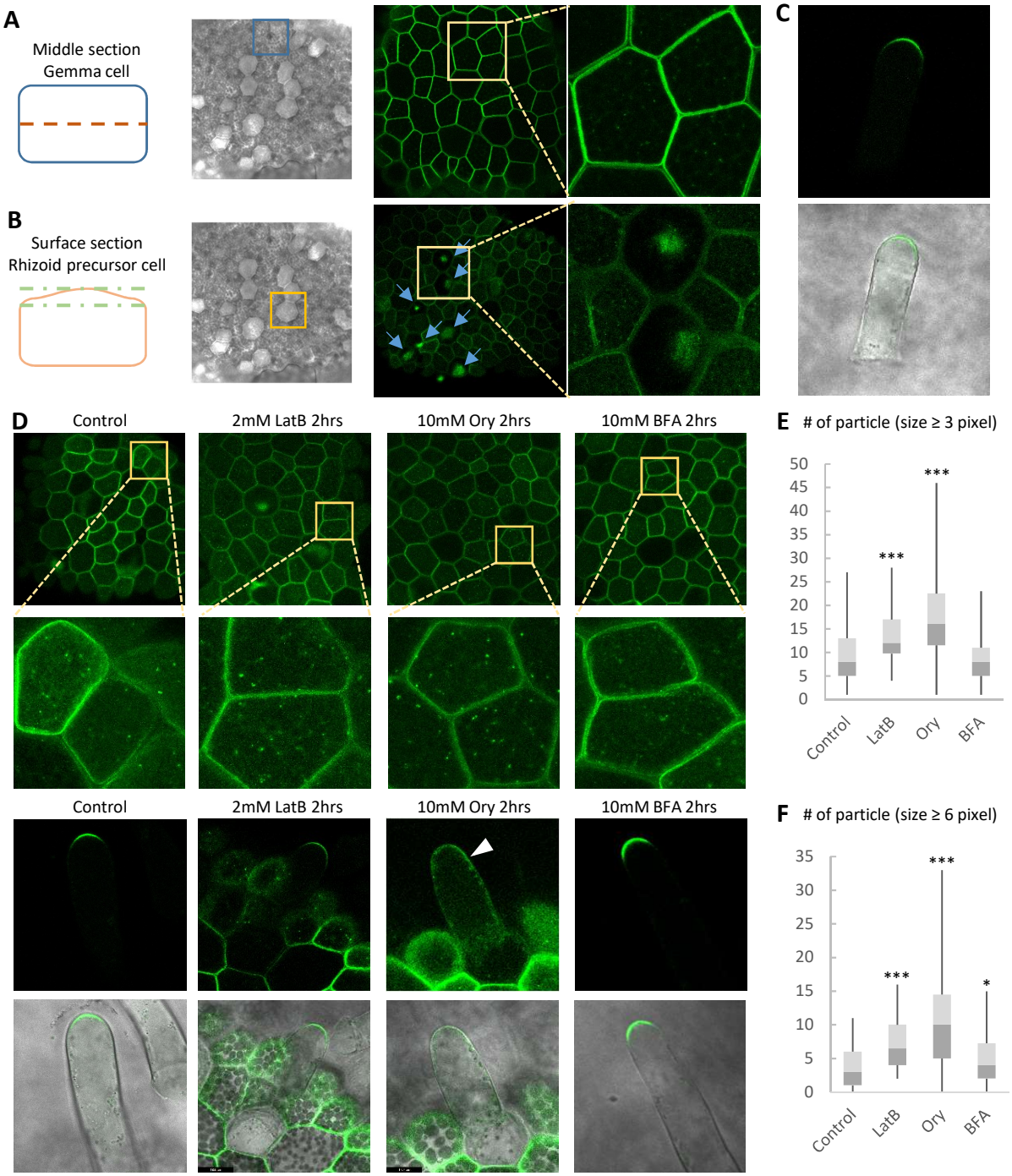

Figure 4. MpPINZ-GFP is only polarized at the tip of young rhizoids in Marchantia.

A – C, The localization of MpPINZ-GFP in gemmae, emerging rhizoids, and young rhizoids.

A, A middle section image as illustrated showing the even distribution of MpPINZ-GFP on the PM of gemmae.

B, Representative image with a 5 µm thick Z-section at the gemma surface as illustrated. Blue arrows indicate the accumulation of MpPINZ-GFP at tips of emerging rhizoids in rhizoid precursor cells.

C, MpPINZ-GFP is polarized at the tip of young rhizoids.

D, The responses of MpPINZ-GFP to indicated treatments. MpPINZ-GFP is localized on the PM with cytosolic puncta signals in gemmae. De-polymerization of cytoskeleton networks caused more and larger cytosolic puncta; BFA treatment resulted in the increase of puncta only with larger size. MpPINZ-GFP is polarized at the tip of young rhizoids, and its polarization was only abolished by Oryzalin treatment (white arrowhead).

E and F, Quantification of intracellular puncta larger than 3 pixels and 6 pixels. 20 cells were quantified in each image, and three images were used to quantify for each treatment (N=60 in total). *P<0.05, **P<0.01, ***P<0.001; Student's *t*-test.

Figure 5. Arabidopsis AtPIN1-GFP is not polarized in Marchantia.

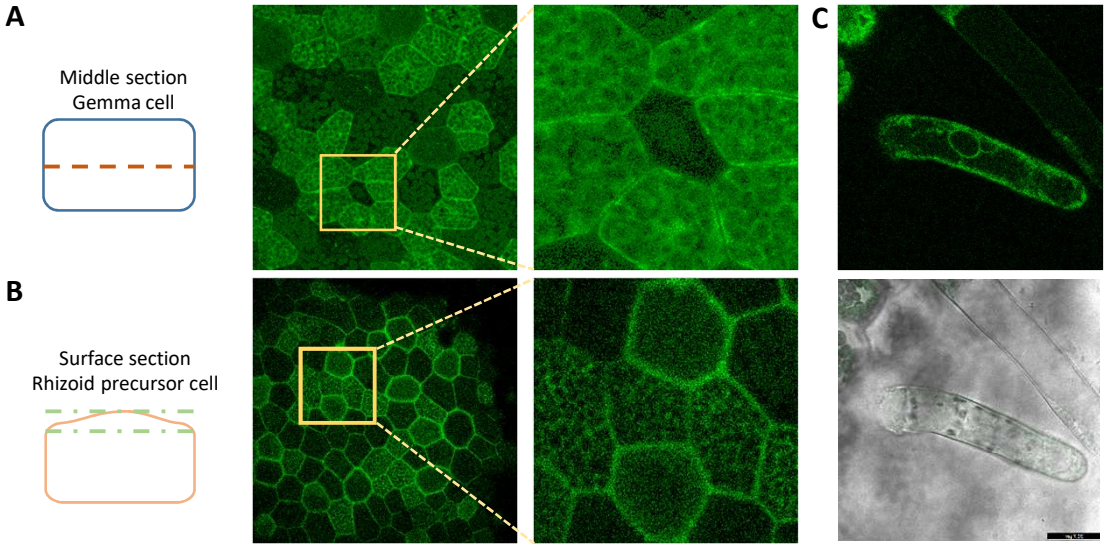

Figure 5. Arabidopsis AtPIN1-GFP is not polarized in Marchantia.

A – C, The localization of AtPIN1-GFP in Marchantia gemmae, emerging rhizoids, and young rhizoids. Imaging sections were obtained as illustrated in A and B. The AtPIN1-GFP is localized on the PM and in the cytoplasm with no apparent puncta signals in all examined tissues.

Figure 6. Overexpression of MpPINZ- and AtPIN-GFPs causes vertical growth of Marchantia thalli.

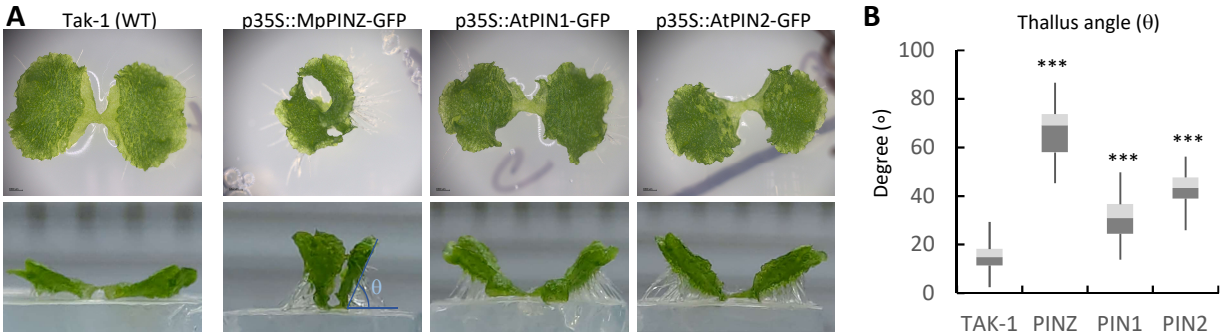

Figure 6. Overexpression of MpPINZ- and AtPIN-GFPs causes vertical growth of Marchantia thalli.

A, Marchantia Tak-1 (WT) expands its thallus horizontally on the agar surface. The overexpression of MpPINZ-, AtPIN1-, and AtPIN2-GFP showed vertical thallus growth, which generated a large angle between the lower surface of the thallus and the surface of the agar (Θ).
B, The quantification of the thallus growth angle (Θ) showed in A. N= 16 – 18 thali for each line. ***P<0.001; Student's *t*-test.

Figure 7. Bryophytic PINs and AtPIN2-GFP utilize different trafficking mechanisms in Arabidopsis epidermal cells.

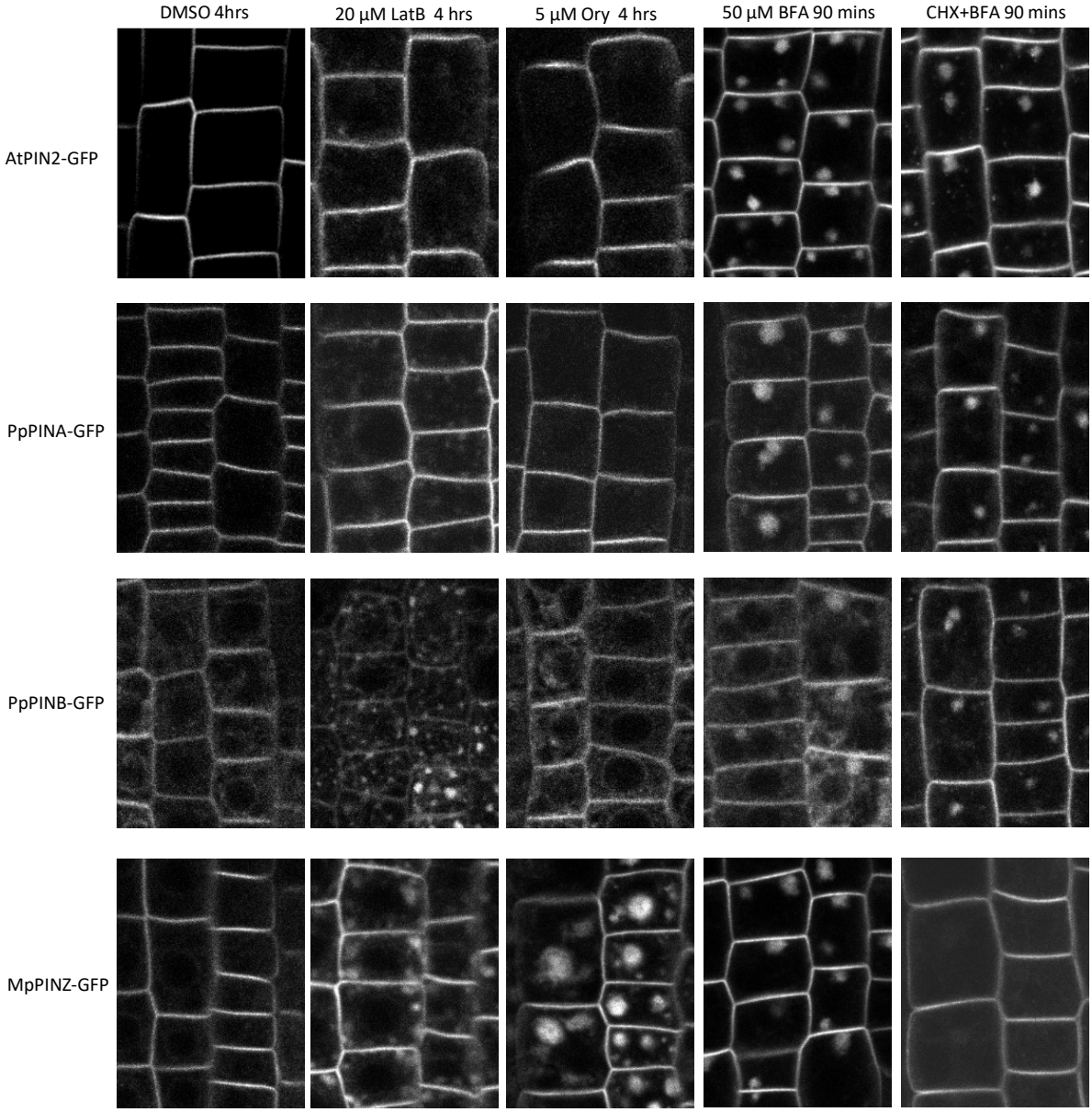

Figure 7. Bryophytic PINs and AtPIN2-GFP utilize different trafficking mechanisms in Arabidopsis epidermal cells.

All PINs were translationally fused with GFP and expressed by the *AtPIN2* promoter. De-polymerization of cytoskeleton networks caused mild internalization of AtPIN2- and PpPINA-GFP, while PpPINB- and MpPINZ-GFP showed strong responses with larger and more intracellular compartments. BFA bodies were observed in all PIN-GFP lines with BFA treatment, while only MpPINZ-GFP showed no BFA bodies in CHX+BFA treatment. Imaging details are described in Methods.

Fig. 8 Bryophytic PINs and AtPIN2-GFP are only polarized to the tip of initial but not elongated root hairs.

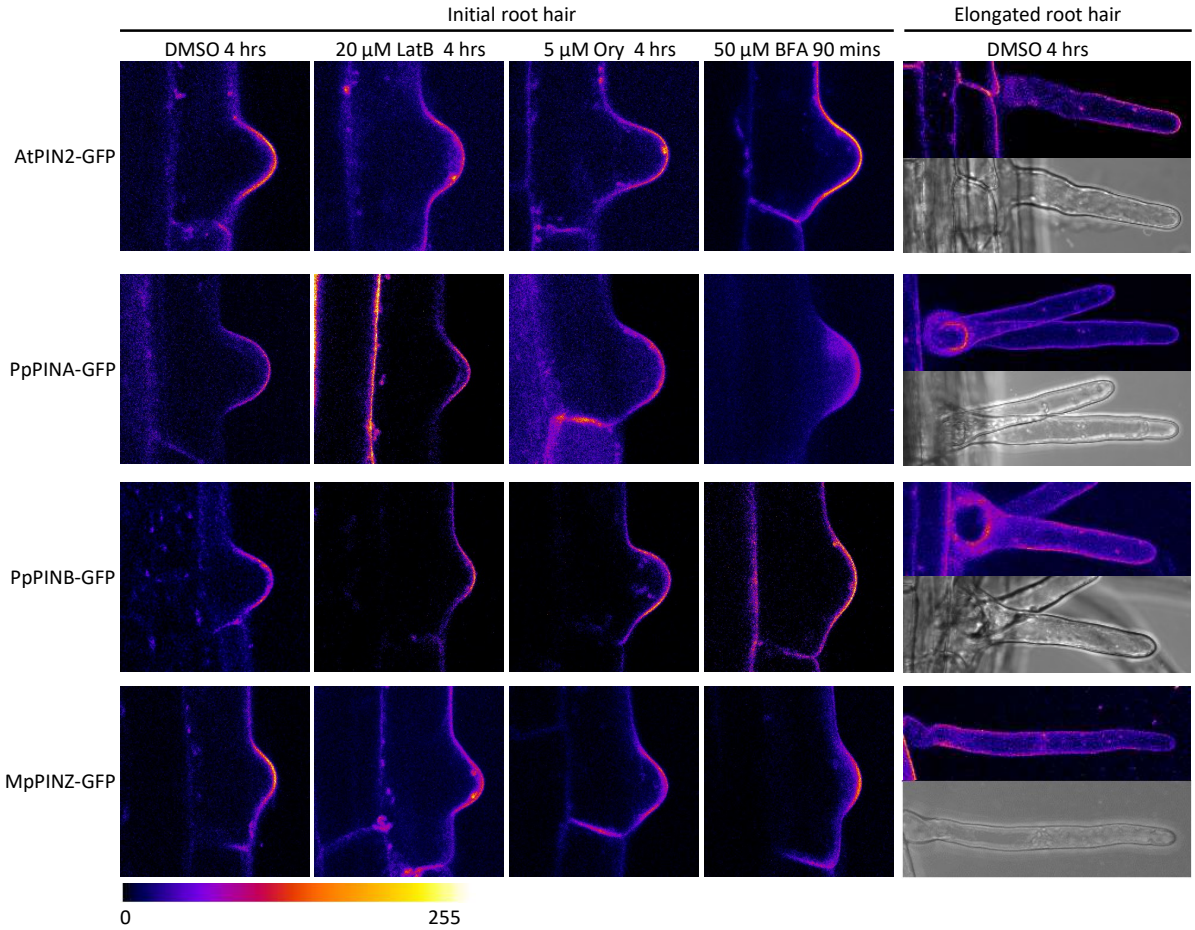

Figure 8. Bryophytic PINs and AtPIN2-GFP are only polarized to the tip of initial but not elongated root hairs.

All PIN-GFP lines show polarized signals at the tip of the initial root hair and none of the indicated treatments disrupted their polarization. Note that the polarization of the PIN-GFP signals were not observed in elongated root hairs. All imaging details are described in Methods. The pixel values ranging from 0 to 255 are represented by the rainbow color.

Parsed Citations

Adamowski, M., and Friml, J. (2015). PIN-dependent auxin transport: action, regulation, and evolution. Plant Cell 27, 20-32.
Google Scholar: Author Only Title Only Author and Title

Baluska, F., Jasik, J., Edelmann, H.G., Salajova, T., and Volkmann, D. (2001). Latrunculin B-induced plant dwarfism: Plant cell elongation is F-actin-dependent. Dev Biol 231, 113-124.
Google Scholar: Author Only Title Only Author and Title

Baskin, T.I., Wilson, J.E., Cork, A., and Williamson, R.E. (1994). Morphology and microtubule organization in Arabidopsis roots exposed to oryzalin or taxol. Plant Cell Physiol 35, 935-942.
Google Scholar: Author Only Title Only Author and Title

Bennett, T.A., Liu, M.M., Aoyama, T., Bierfreund, N.M., Braun, M., Coudert, Y., Dennis, R.J., O'Connor, D., Wang, X.Y., White, C.D., Decker, E.L., Reski, R., and Harrison, C.J. (2014). Plasma membrane-targeted PIN proteins drive shoot development in a moss. Curr Biol 24, 2776-2785.
Google Scholar: Author Only Title Only Author and Title

Blazquez, M.A., Nelson, D.C., and Weijers, D. (2020). Evolution of Plant Hormone Response Pathways. Annu Rev Plant Biol 71, 327-353.
Google Scholar: Author Only Title Only Author and Title

Dhonukshe, P., Aniento, F., Hwang, I., Robinson, D.G., Mravec, J., Stierhof, Y.D., and Friml, J. (2007). Clathrin-mediated constitutive endocytosis of PIN auxin efflux carriers in Arabidopsis. Curr Biol 17, 520-527.
Google Scholar: Author Only Title Only Author and Title

Era, A., Kutsuna, N., Higaki, T., Hasezawa, S., Nakano, A., and Ueda, T. (2013). Microtubule stability affects the unique motility of F-actin in Marchantia polymorpha. J Plant Res 126, 113-119.
Google Scholar: Author Only Title Only Author and Title

Floriach-Clark, J., Tang, H., and Willemsen, V. (2021). Mosses: Accessible Systems for Plant Development Studies. In Model Organisms in Plant Genetics (IntechOpen.
Google Scholar: Author Only Title Only Author and Title

Friml, J. (2021). Fourteen Stations of Auxin. Cold Spring Harb Perspect Biol 14, a039859.
Google Scholar: Author Only Title Only Author and Title

Geldner, N., Friml, J., Stierhof, Y.D., Jurgens, G., and Palme, K. (2001). Auxin transport inhibitors block PIN1 cycling and vesicle trafficking. Nature 413, 425-428.
Google Scholar: Author Only Title Only Author and Title

Glanc, M., Fendrych, M., and Friml, J. (2018). Mechanistic framework for cell-intrinsic re-establishment of PIN2 polarity after cell division. Nat Plants 4, 1082-1088.
Google Scholar: Author Only Title Only Author and Title

Glanc, M., Fendrych, M., and Friml, J. (2019). PIN2 Polarity Establishment in Arabidopsis in the Absence of an Intact Cytoskeleton. Biomolecules 9, 222.
Google Scholar: Author Only Title Only Author and Title

Ishizaki, K., Nishihama, R., Ueda, M., Inoue, K., Ishida, S., Nishimura, Y., Shikanai, T., and Kohchi, T. (2015). Development of Gateway Binary Vector Series with Four Different Selection Markers for the Liverwort Marchantia polymorpha. PLoS One 10, e0138876.
Google Scholar: Author Only Title Only Author and Title

Kato, H., Nishihama, R., Weijers, D., and Kohchi, T. (2018). Evolution of nuclear auxin signaling: lessons from genetic studies with basal land plants. J Exp Bot 69, 291-301.
Google Scholar: Author Only Title Only Author and Title

Kleine-Vehn, J., Langowski, L., Wisniewska, J., Dhonukshe, P., Brewer, P.B., and Friml, J. (2008a). Cellular and molecular requirements for polar PIN targeting and transcytosis in plants. Mol Plant 1, 1056-1066.
Google Scholar: Author Only Title Only Author and Title

Kleine-Vehn, J., Dhonukshe, P., Sauer, M., Brewer, P.B., Wisniewska, J., Paciorek, T., Benkova, E., and Friml, J. (2008b). ARF GEF-dependent transcytosis and polar delivery of PIN auxin carriers in Arabidopsis. Curr Biol 18, 526-531.
Google Scholar: Author Only Title Only Author and Title

Kleine-Vehn, J., Wabnik, K., Martiniere, A., Langowski, L., Willig, K., Naramoto, S., Leitner, J., Tanaka, H., Jakobs, S., Robert, S., Luschnig, C., Govaerts, W., Hell, S.W., Runions, J., and Friml, J. (2011). Recycling, clustering, and endocytosis jointly maintain PIN auxin carrier polarity at the plasma membrane. Mol Syst Biol 7, 540.
Google Scholar: Author Only Title Only Author and Title

Krecek, P., Skupa, P., Libus, J., Naramoto, S., Tejos, R., Friml, J., and Zazimalova, E. (2009). The PIN-FORMED (PIN) protein family of auxin transporters. Genome Biol 10, 249.
Google Scholar: Author Only Title Only Author and Title

Kubo, M., Imai, A., Nishiyama, T., Ishikawa, M., Sato, Y., Kurata, T., Hiwatashi, Y., Reski, R., and Hasebe, M. (2013). System for stable beta-estradiol-inducible gene expression in the moss Physcomitrella patens. PLoS One 8, e77356.
Google Scholar: Author Only Title Only Author and Title

Kubota, A., Ishizaki, K., Hosaka, M., and Kohchi, T. (2013). Efficient Agrobacterium-mediated transformation of the liverwort Marchantia polymorpha using regenerating thalli. Biosci Biotechnol Biochem 77, 167-172.
Google Scholar: Author Only Title Only Author and Title

Lavy, M., Prigge, M.J., Tao, S., Shain, S., Kuo, A., Kirchsteiger, K., and Estelle, M. (2016). Constitutive auxin response in Physcomitrella reveals complex interactions between Aux/IAA and ARF proteins. Elife 5, e13325.
Google Scholar: Author Only Title Only Author and Title

Leyser, O. (2018). Auxin Signaling. Plant Physiol 176, 465-479.
Google Scholar: Author Only Title Only Author and Title

Li, H., von Wangenheim, D., Zhang, X., Tan, S., Darwish-Miranda, N., Naramoto, S., Wabnik, K., De Rycke, R., Kaufmann, W.A., Gutl, D., Tejos, R., Grones, P., Ke, M., Chen, X., Dettmer, J., and Friml, J. (2021). Cellular requirements for PIN polar cargo clustering in Arabidopsis thaliana. New Phytol 229, 351-369.
Google Scholar: Author Only Title Only Author and Title

Mockaitis, K., and Estelle, M. (2008). Auxin receptors and plant development: a new signaling paradigm. Annu Rev Cell Dev Biol 24, 55-80.
Google Scholar: Author Only Title Only Author and Title

Nakaoka, Y., Miki, T., Fujioka, R., Uehara, R., Tomioka, A., Obuse, C., Kubo, M., Hiwatashi, Y., and Goshima, G. (2012). An inducible RNA interference system in Physcomitrella patens reveals a dominant role of augmin in phragmoplast microtubule generation. Plant Cell 24, 1478-1493.
Google Scholar: Author Only Title Only Author and Title

Naramoto, S., Otegui, M.S., Kutsuna, N., de Rycke, R., Dainobu, T., Karampelias, M., Fujimoto, M., Feraru, E., Miki, D., Fukuda, H., Nakano, A., and Friml, J. (2014). Insights into the localization and function of the membrane trafficking regulator GNOM ARF-GEF at the Golgi apparatus in Arabidopsis. Plant Cell 26, 3062-3076.
Google Scholar: Author Only Title Only Author and Title

Narasimhan, M., Gallei, M., Tan, S., Johnson, A., Verstraeten, I., Li, L., Rodriguez, L., Han, H., Himschoot, E., Wang, R., Vanneste, S., Sanchez-Simarro, J., Aniento, F., Adamowski, M., and Friml, J. (2021). Systematic analysis of specific and nonspecific auxin effects on endocytosis and trafficking. Plant Physiol 186, 1122-1142.
Google Scholar: Author Only Title Only Author and Title

Nishiyama, T., Hiwatashi, Y., Sakakibara, I., Kato, M., and Hasebe, M. (2000). Tagged mutagenesis and gene-trap in the moss, Physcomitrella patens by shuttle mutagenesis. DNA Res 7, 9-17.
Google Scholar: Author Only Title Only Author and Title

Oda, Y., Hirata, A., Sano, T., Fujita, T., Hiwatashi, Y., Sato, Y., Kadota, A., Hasebe, M., and Hasezawa, S. (2009). Microtubules regulate dynamic organization of vacuoles in Physcomitrella patens. Plant Cell Physiol 50, 855-868.
Google Scholar: Author Only Title Only Author and Title

Otani, K., Ishizaki, K., Nishihama, R., Takatani, S., Kohchi, T., Takahashi, T., and Motose, H. (2018). An evolutionarily conserved NIMA-related kinase directs rhizoid tip growth in the basal land plant Marchantia polymorpha. Development 145, dev154617.
Google Scholar: Author Only Title Only Author and Title

Rensing, S.A., Goffinet, B., Meyberg, R., Wu, S.Z., and Bezanilla, M. (2020). The Moss Physcomitrium (Physcomitrella) patens: A Model Organism for Non-Seed Plants. Plant Cell 32, 1361-1376.
Google Scholar: Author Only Title Only Author and Title

Sauer, M., and Kleine-Vehn, J. (2019). PIN-FORMED and PIN-LIKES auxin transport facilitators. Development 146, dev.168088.
Google Scholar: Author Only Title Only Author and Title

Schlink, K., and Reski, R. (2002). Preparing high-quality DNA from moss (Physcomitrella patens). Plant Molecular Biology Reporter 20, 423-423.
Google Scholar: Author Only Title Only Author and Title

Shimamura, M. (2016). Marchantia polymorpha: Taxonomy, Phylogeny and Morphology of a Model System. Plant Cell Physiol 57, 230-256.
Google Scholar: Author Only Title Only Author and Title

Skokan, R., Medvecka, E., Viaene, T., Vosolsobe, S., Zwiewka, M., Muller, K., Skupa, P., Karady, M., Zhang, Y., Janacek, D.P., Hammes, U.Z., Ljung, K., Nodzynski, T., Petrasek, J., and Friml, J. (2019). PIN-driven auxin transport emerged early in streptophyte evolution. Nat Plants 5, 1114-1119.
Google Scholar: Author Only Title Only Author and Title

Smit, M.E., and Weijers, D. (2015). The role of auxin signaling in early embryo pattern formation. Curr Opin Plant Biol 28, 99-105.
Google Scholar: Author Only Title Only Author and Title

Steinmann, T., Geldner, N., Grebe, M., Mangold, S., Jackson, C.L., Paris, S., Galweiler, L., Palme, K., and Jurgens, G. (1999). Coordinated polar localization of auxin efflux carrier PIN1 by GNOM ARF GEF. Science 286, 316-318.
Google Scholar: Author Only Title Only Author and Title

Tang, H., Duijts, K., Bezanilla, M., Scheres, B., Vermeer, J.E.M., and Willemsen, V. (2020). Geometric cues forecast the switch from two- to three-dimensional growth in Physcomitrella patens. New Phytol 225, 1945-1955.
Google Scholar: Author Only Title Only Author and Title

Tao, S., and Estelle, M. (2018). Mutational studies of the Aux/IAA proteins in Physcomitrella reveal novel insights into their function. New Phytol 218, 1534-1542.
Google Scholar: Author Only Title Only Author and Title

Vanneste, S., and Friml, J. (2009). Auxin: a trigger for change in plant development. Cell 136, 1005-1016.
Google Scholar: Author Only Title Only Author and Title

Viaene, T., Landberg, K., Thelander, M., Medvecka, E., Pederson, E., Feraru, E., Cooper, E.D., Karimi, M., Delwiche, C.F., Ljung, K., Geisler, M., Sundberg, E., and Friml, J. (2014). Directional auxin transport mechanisms in early diverging land plants. Curr Biol 24, 2786-2791.
Google Scholar: Author Only Title Only Author and Title

Vidali, L., Rounds, C.M., Hepler, P.K., and Bezanilla, M. (2009). Lifeact-mEGFP reveals a dynamic apical F-actin network in tip growing plant cells. PLoS One 4, e5744.
Google Scholar: Author Only Title Only Author and Title

Vieten, A., Vanneste, S., Wisniewska, J., Benkova, E., Benjamins, R., Beeckman, T., Luschnig, C., and Friml, J. (2005). Functional redundancy of PIN proteins is accompanied by auxin-dependent cross-regulation of PIN expression. Development 132, 4521-4531.
Google Scholar: Author Only Title Only Author and Title

Yamada, M., Miki, T., and Goshima, G. (2016). Imaging Mitosis in the Moss Physcomitrella patens. Methods Mol Biol 1413, 263-282.
Google Scholar: Author Only Title Only Author and Title

Yu, Z., Zhang, F., Friml, J., and Ding, Z. (2022). Auxin signaling: Research advances over the past 30 years. J Integr Plant Biol 64, 371-392.
Google Scholar: Author Only Title Only Author and Title

Zhang, Y., Xiao, G., Wang, X., Zhang, X., and Friml, J. (2019). Evolution of fast root gravitropism in seed plants. Nat Commun 10, 3480.
Google Scholar: Author Only Title Only Author and Title

Zourelidou, M., Absmanner, B., Weller, B., Barbosa, I.C., Willige, B.C., Fastner, A., Streit, V., Port, S.A., Colcombet, J., de la Fuente van Bentem, S., Hirt, H., Kuster, B., Schulze, W.X., Hammes, U.Z., and Schwechheimer, C. (2014). Auxin efflux by PIN-FORMED proteins is activated by two different protein kinases, D6 PROTEIN KINASE and PINOID. Elife 3, e02860.
Google Scholar: Author Only Title Only Author and Title